

AD-A133 761

ANALYSIS OF THE NONLINEAR LARGE DEFORMATION BEHAVIOR OF 1//
COMPOSITE CYLINDR..(U) GEORGIA INST OF TECH ATLANTA
SCHOOL OF ENGINEERING SCIENCE AN.. G J SIMITSES ET AL.
1983 AFOSR-TR-83-0870 AFOSR-81-0227 F/G 20/11 NL

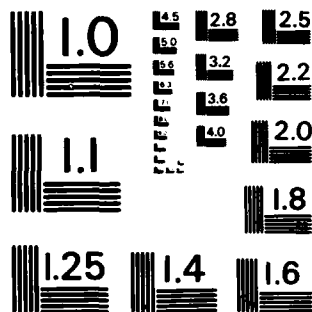
UNCLASSIFIED

END

DATE
FILMED

1 11

DTIC



MICROCOPY RESOLUTION TEST CHART
NATIONAL BUREAU OF STANDARDS-1963-A

AD-A 133761

ANALYSIS OF THE NONLINEAR BUCKLING BEHAVIOR OF COMPOSITE CYLINDRICAL SHELLS

George J. Simionescu

Initial Statement

and

Dein Shaw



DTIC
STANDARD

DTIC COPY

Office of Naval Research
Contract N00019-79-1-0001
Awardee: Naval Research Laboratory
Durham, North Carolina

Qualified requestors may obtain additional copies from the Defense Documentation Center, all others should apply to the National Technical Information Service

UNCLASSIFIED

SECURITY CLASSIFICATION OF THIS PAGE (When Data Entered)

REPORT DOCUMENTATION PAGE		READ INSTRUCTIONS BEFORE COMPLETING FORM
1. REPORT NUMBER AFOSR-TR- 83-0870	2. GOVT ACCESSION NO. AD-A133761	3. RECIPIENT'S CATALOG NUMBER
4. TITLE (and Subtitle) ANALYSIS OF THE NONLINEAR LARGE DEFORMATION BEHAVIOR OF COMPOSITE CYLINDRICAL SHELLS		5. TYPE OF REPORT & PERIOD COVERED Final June 30, 1981 - June 30, 1983
7. AUTHOR(s) George J. Simitzes Izhak Sheinman and Dein Shaw		8. CONTRACT OR GRANT NUMBER(s) AFOSR 81-0227
9. PERFORMING ORGANIZATION NAME AND ADDRESS Georgia Institute of Technology School of Engineering Science and Mechanics 225 North Ave., N.W. Atlanta, GA 30332		10. PROGRAM ELEMENT, PROJECT, TASK AREA & WORK UNIT NUMBERS 2307/B1 61102F
11. CONTROLLING OFFICE NAME AND ADDRESS Air Force Office of Scientific Research/NA Bldg. 410 Bolling AFB, D.C. 20332		12. REPORT DATE 1983
14. MONITORING AGENCY NAME & ADDRESS (if different from Controlling Office)		13. NUMBER OF PAGES 88
		15. SECURITY CLASS. (of this report) Unclassified
		15a. DECLASSIFICATION/DOWNGRADING SCHEDULE
16. DISTRIBUTION STATEMENT (of this Report) Approved for public release; distribution unlimited		
17. DISTRIBUTION STATEMENT (of the abstract entered in Block 20, if different from Report)		
18. SUPPLEMENTARY NOTES		
19. KEY WORDS (Continue on reverse side if necessary and identify by block number) Composite Cylinders Axial Compression Laminated Shells Torsion Stability Nonlinear Shell Theories Stiffened Shells		
20. ABSTRACT (Continue on reverse side if necessary and identify by block number) The governing equations for the nonlinear analysis of imperfect, stiffened, laminated, circular, cylindrical, thin shells, subjected to uniform axial compression and torsion, and supported in various ways, are derived and presented. Two types of formulations have been developed; one (w,F-Formulation) is based Donnell-type nonlinear kinematic relations; and the other (u,v,w - formulation) is based on Sanders'-type of nonlinear kinematic relations (small strains, moderate rotations about in-plane axes).		

DD FORM 1473

JAN 73

EDITION OF 1 NOV 65 IS OBSOLETE

UNCLASSIFIED

SECURITY CLASSIFICATION OF THIS PAGE (When Data Entered)

UNCLASSIFIED

SECURITY CLASSIFICATION OF THIS PAGE (When Data Entered)

A solution methodology is developed and presented. Numerical results are generated for certain special geometries, and these serve as bench marks for the solution scheme. Parametric studies are performed for composite cylinders. The scope of these studies is to assess the effect of (a) geometric imperfections (b) lamina stacking, and (c) length to radius ratio. The solution scheme is also tested by comparing theoretical predictions (critical loads based on the developed methodology) to experimentally obtained results.

UNCLASSIFIED

SECURITY CLASSIFICATION OF THIS PAGE (When Data Entered)

ANALYSIS OF THE NONLINEAR LARGE DEFORMATION
BEHAVIOR OF COMPOSITE CYLINDRICAL SHELLS*

by



George J. Simitzes⁺, Dein Shaw⁺⁺

and

Izhak Sheinmann⁺⁺⁺

Georgia Institute of Technology

Accession For	
NTIS	<input checked="" type="checkbox"/>
DTIC	<input type="checkbox"/>
Unannounced	<input type="checkbox"/>
Justification	
By	
Distribution/	
Availability Codes	
Dist	Avail and/or Special
A	

*This work was supported by the United States Air Force Office of Scientific Research under Grant AFOSR-81-0227

⁺Professor of Engineering Science and Mechanics

⁺⁺Postdoctoral Fellow, School of Engineering Science and Mechanics

⁺⁺⁺Visiting Scholar; on leave from Israel Institute of Technology, Haifa, Israel

Qualified requestors may obtain additional copies from the Defense Documentation Center, all others should apply to the National Technical Information Service.

Conditions of Reproduction

Reproduction, translation, publication, use and disposal in whole or in part for the United States Government is permitted.

AIR FORCE OFFICE OF SCIENTIFIC RESEARCH (AFOSR)
NOTICE OF TRANSMITTAL TO DTIC

This technical report has been reviewed and is approved for public release 17W APR 198-12.

Distribution is unlimited.

MATTHEW J. KERPER

Chief, Technical Information Division

TABLE OF CONTENTS

	<u>Page</u>
NOMENCLATURE	ii
SUMMARY	iv
CHAPTER	
I. INTRODUCTION	
II. MATHEMATICAL FORMULATION AND SOLUTION	
III. RESULTS AND DISCUSSION; u, v, w - FORMULATION	
III.1 Description of Structural Geometry	
III.2 Numerical Results	
III.3 Comparison with Experimental Data	
III.4 Concluding Remarks	
IV. ADDITIONAL RESULTS; w, F - FORMULATION	
IV.1 Description of Geometry	
IV.2 Discussion of Results	
IV.3 Comparison with Experimental Data	
IV.4 Concluding Remarks	
V. CONCLUSIONS AND RECOMMENDATIONS	
REFERENCES	

NOMENCLATURE

A_x, A_y	= Stiffener Cross-Sectional Areas
A_{ij}	$= \sum_{k=1}^N \bar{Q}_{ij}^k (z_k - z_{k-1})$
B_{ij}	$= \frac{1}{2} \sum_{k=1}^N \bar{Q}_{ij}^k (z_k^2 - z_{k-1}^2)$
D_{ij}	$= \frac{1}{3} \sum_{k=1}^N \bar{Q}_{ij}^k (z_k^3 - z_{k-1}^3)$
$E_{11}, E_{22}, G_{12}, \nu_{12}$	= Orthotropic Material Engineering Constants
E_x, E_y	= Young's Moduli for Stiffener Material
e_x, e_y	= Stiffener Eccentricities
F	= Airy Stress Function
h	= Shell Thickness
h_n, h_o	= z-Coordinate of Extreme Surfaces of the Shell
I_{x_c}, I_{y_c}	= Second Moments of Stiffener Areas
L	= Length of Shell
l_x, l_y	= Stiffener Spacings
M_{xx}, M_{xy}, M_{yy}	= Moment Resultants
N_{xx}, N_{xy}, N_{yy}	= Stress Resultants
$\bar{N}_{xx}, \bar{N}_{xy}$	= Applied Stress Resultants
\bar{Q}_{ij}	= Material Elastic Constant
R	= Radius of Shell
u, v, w	= Displacement Components
w^0	= Initial Geometric Imperfection

NOMENCLATURE (Continued)

x, y, z	= Coordinates
Z	= Batdorf Curvature Parameter
δ_1	= 0 for Donnell's Approximation = 1 for Sanders' Approximation
$\epsilon_{xx}^o, \epsilon_{xy}^o, \epsilon_{yy}^o$	= Reference Surface Strain Components
θ	= Angle Between the Strong Orthotropic Direction and the x-axis
$\kappa_{xx}, \kappa_{yy}, \kappa_{xy}$	= Changes of Curvatures and Torsion of Reference Surface
ξ	= Imperfection Amplitude Parameter
$\sigma_{xx}, \sigma_{yy}, \sigma_{xy}$	= Stress Components
φ_x, φ_y	= Rotations About In-plane Axes x and y

SUMMARY

Imperfect, laminated, circular, cylindrical, thin shells supported in various ways and subjected to a uniform axial compression and torsion (individually applied or in combination) are analyzed. The analysis is based on nonlinear kinematic relations, linearly elastic material behavior, and the usual lamination theory. The laminate consists of orthotropic laminae, which typically characterize fiber reinforced composites. Two types of formulation have been developed; one is referred to as the w, F -formulation, based on Donnell-type of kinematic relations. The governing equations consist of the transverse equilibrium equation and the in-plane compatibility equation. These two equations are expressed in terms of the transverse displacement, w , and an airy stress resultant function, F . The other, referred to as the u, v, w -formulation, is based on Sanders'-type of kinematic relations. The governing equations for this case consist of the three equilibrium equations. These three equations are expressed in terms of two in-plane displacement components u, v , and the transverse displacement component, w . Donnell's type of shell theory approximation can be treated as a special case in the u, v, w -formulation.

Some results are generated for certain geometries (isotropic and laminated) and these serve as bench marks for the solution scheme (both formulations). Results are also generated for composite cylinders by changing several parameters. The scope of these parametric studies is to establish the effect of geometric imperfections, lamina stacking, and length to radius ratio. Moreover, theoretically computed critical conditions are compared to experimentally obtained results.

CHAPTER I

INTRODUCTION

Shell configurations of various constructions (metallic with or without stiffeners, laminated, plastic etc.) have been widely used as structural elements, for many decades. These configurations, in many cases, are primarily designed to withstand destabilizing loads, which are applied individually or in combination. Various linear and nonlinear shell theories (based on different approximations of the kinematic relations) have been employed in attempting to predict critical loads, as well as, pre- and post-buckling behavior of perfect and imperfect shell configurations.

One of the simplest shell theories is that, which is based on the Donnell (1) approximation (or Mushtari-Vlasov-Donnell approximation) for both, linear and nonlinear kinematic relations. Donnell's equations have been widely used in the solution of problems of stability and equilibrium.

From time to time, because of the approximate nature and because of the extreme simplicity of Donnell's equations, doubt has been raised as to their accuracy. Hoff (2) in 1955 gave the range of some basic parameters of perfect, thin, circular, cylindrical shells, for which solutions to Donnell's and Flügge's (3) equations are approximately equal. Moreover, Dym (4) in 1973 compared buckling results obtained from Donnell's equations with those obtained from Koiter-Budiansky (5,6) equations for thin, circular, perfect cylinders in uniform axial compression. Furthermore, Simites and Aswani (7) compared critical loads for the entire range of radius to thickness and length to radius ratios and for various load behaviors (during the buckling process for a laterally loaded thin cylindrical shell

by employing several linear shell theories; Koiter-Budiansky (5,6), Sanders (8), Flügge (3) and Donnell (1).

Other comparisons of the linear version of the various shell theories have been reported by Toda (9), Koga and Endo (10), Microys and Schwaighofer (11, 12) and Akeju (13). All of the above investigations deal with isotropic thin cylindrical shells except for Ref. 12, which deals with an orthotropic cylindrical shell.

The only investigation that has any nonlinear flavor is the study of El Naschie and Hosni (14), but even this deals only with initial post-buckling behavior and for an infinitely long thin cylinder (thin ring).

The present report gives a comparison between critical loads for imperfect, thin, cylindrical shells (limit point loads) of isotropic and composite construction, under uniform axial compression for two shell theories, that of Sanders (8) and that of Donnell (1). The intention here is to identify the parameters which affect the accuracy of critical conditions established through Donnell equations, by comparing them to those established by Sanders equations. The implication here is that the Sanders equations, which are typical of the more accurate nonlinear shell equations (5,6,7), should yield accurate results, while the Donnell equations are viewed as approximate and therefore less accurate.

This report is a continuation of Ref. 15. In Ref. 15 the following are presented: 1) the mathematical formulation and derivation of the governing equations, based on Donnell-type (1) non-linear kinematic relations, and presented in terms of the transverse displacement component, w , and an Airy stress (resultant) function, F , defined in the text; this is called the w, F - formulation; 2) the mathematical formulation and deriva-

tion of the governing equations, base on Sanders-type (8) nonlinear kinematic relations and presented in terms of the three displacement components, u , v and w ; the kinematic relations used correspond to small strains, small rotations about the normal, but moderate rotations about in-plane axes; this is called the u,v,w -formulation, and the Donnell's kinematic relations are included in the Sanders relations, therefore this formulation covers both cases (Donnell is a special case of the Sanders equations); 3) solution schemes for both formulations; the solution methodology for the w , F -formulation includes the capability of obtaining post-limit point behavior, while the solution scheme for the u,v,w - formulation refers only to pre-limit point behavior (but nonlinear) including the estimation of critical conditions (limit point loads); moreover, the flow chart and listing of the respective computer codes are presented in the appendices of Ref. 15; 4) several numerical results, generated with two objectives in mind, (a) some serve as bench marks for the solution schemes, and (b) some limited parametric studies are performed in order to assess effects of boundary conditions, of load eccentricity and of lamina stacking sequence for axially-loaded laminated cylindrical shells. Furthermore, some limited studies are performed for torsion. For both load cases, the imperfection sensitivity of the configuration is assessed; all of these results were obtained by employing the w,F -formulation.

In this report, additional results, obtained by the w,F -formulation, are presented. The objective here is to compare theoretical predictions with experimental results. Moreover, results (critical conditions), obtained by the u,v,w -formulation are presented. The objective here is to

establish which parameters affect the accuracy of Donnell-type of equations. This is accomplished by comparing Donnell-theory results with Sanders-theory results, the implication being here that the Sanders-theory results are closer to being exact. This is done for axially-loaded, imperfect shells of isotropic, orthotropic and laminated construction. These studies are necessary in order to establish the acceptability of the parametric studies (conclusions of) presented in Ref. 15. Finally, since the reported studies are not complete, proper recommendations are offered.

CHAPTER II

MATHEMATICAL FORMULATION AND SOLUTION

The mathematical formulation and a concise description of the solution scheme, for the u,v,w -formulation are presented in this chapter. The geometry and sign convention are shown on Figs. 1 and 2. The configuration consists of a laminate, which is orthogonally and eccentrically (in general) stiffened by closely spaced stiffeners (in the axial and hoop directions of the cylinder).

In this formulation (u,v,w), two distinctly different kinematic relations (different shell theories) are employed. One is due to Sanders (8) and one due to Donnell (1). In the case of Sanders' equations it is assumed that the reference surface strains are small, the rotation about the normal is negligibly small and the rotations about in-plane axes are moderate.

II.1 Kinematic Relations

The Sanders kinematic relations are based on the assumption of a perfect reference surface (in our case perfectly circular, cylindrical surface). These kinematic relations are modified to include the effect of a small initial geometric imperfection, $w^0(x,y)$.

Let $w^0(x,y)$ be measured from the perfectly cylindrical surface of the laminated shell. Let $w(x,y)$ denote the transverse displacement component of material points on the reference surface and be measured from the undeformed surface. It is positive outward (see Fig. 1) and the midsurface of the laminate is taken to be the reference surface (for convenience; the choice is arbitrary). Let $u(x,y)$ and $v(x,y)$ be the in-plane displacement

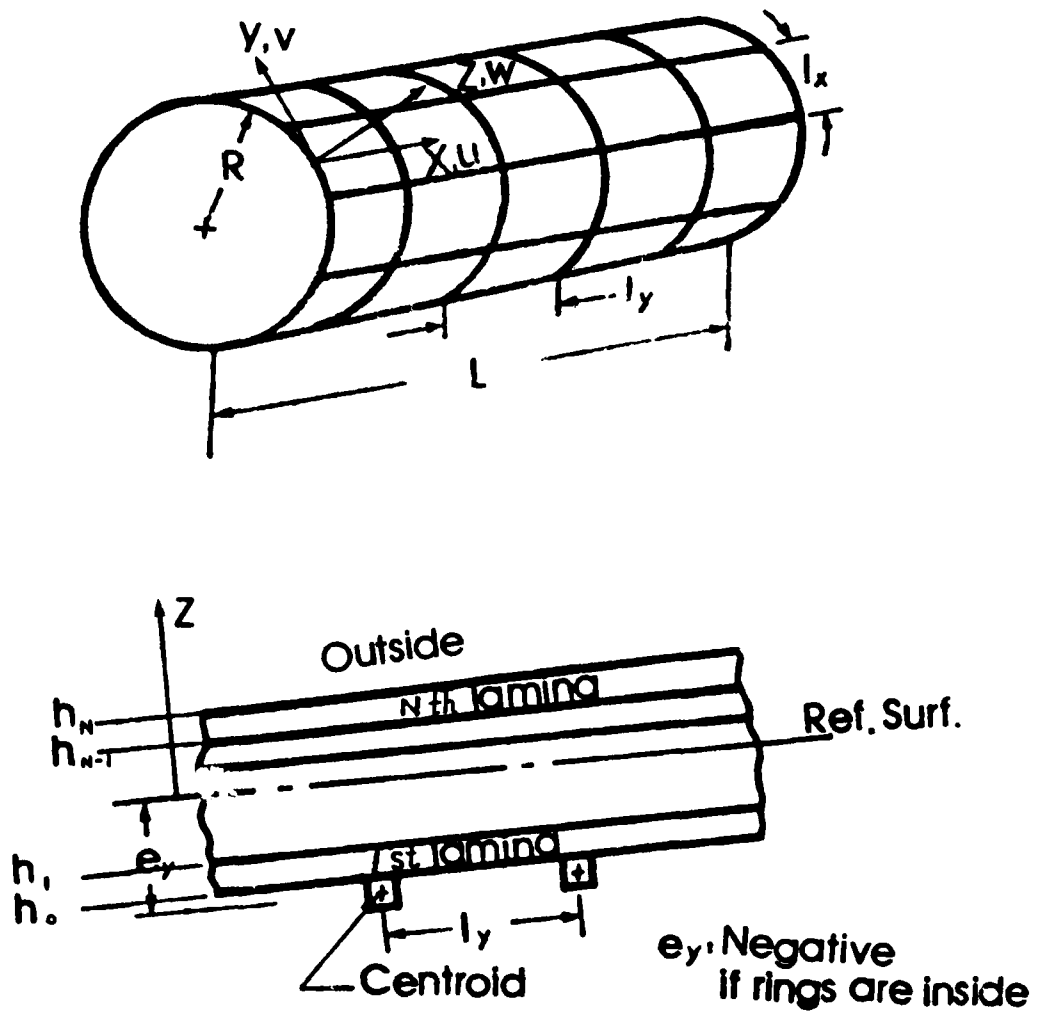
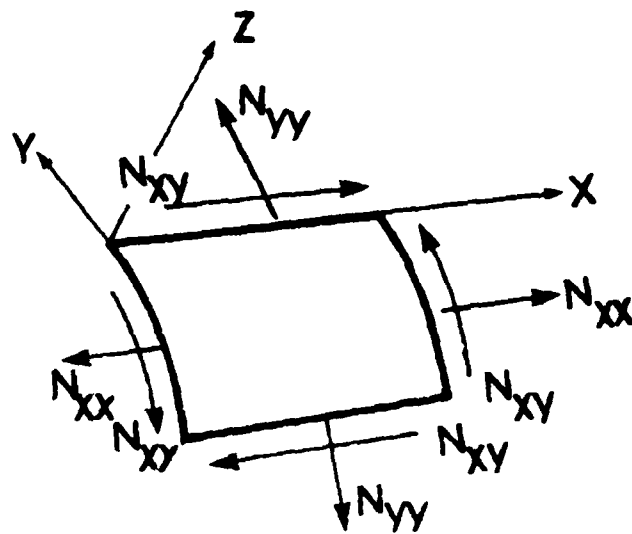
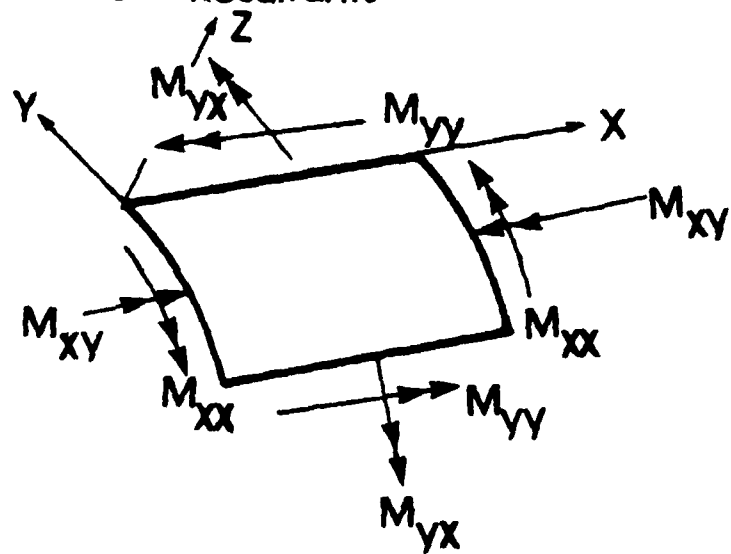


Fig. 1 Geometry and Sign Convention



Stress Resultants



Moment Resultants

Fig. 2. Stress and Moment Resultants
(Right Hand Rule)

components (see Fig. 1). The kinematic or strain-displacement relations are:

$$\epsilon_{xx} = \epsilon_{xx}^0 + z \kappa_{xx}; \quad \epsilon_{yy} = \epsilon_{yy}^0 + z \kappa_{yy}; \quad \gamma_{xy} = \gamma_{xy}^0 + 2z \kappa_{xy} \quad (1)$$

where

$$\left. \begin{aligned} \epsilon_{xx}^0 &= u_{,x} + \frac{1}{2} w_{,x}^2 + w_{,x} w_{,x}^0 \\ \epsilon_{yy}^0 &= v_{,y} + \frac{w}{R} + \frac{1}{2} w_{,y}^2 + w_{,y} w_{,y}^0 + \frac{\delta_1}{2} \left[\frac{v^2}{R^2} - 2 \frac{v}{R} (w_{,y} + w_{,y}^0) \right] \\ \gamma_{xy}^0 &= u_{,y} + v_{,x} + w_{,x} w_{,y} + w_{,x}^0 w_{,y} + w_{,x} w_{,y}^0 - \delta_1 \left[\frac{v}{R} (w_{,y} + w_{,y}^0) \right] \end{aligned} \right\} \quad (2)$$

$$\phi_x = -w_{,x} \quad ; \quad \phi_y = -w_{,y} + \delta_1 \left(\frac{v}{R} \right) \quad (3)$$

$$\kappa_{xx} = -w_{,xx}; \quad \kappa_{yy} = -w_{,yy} + \delta_1 \left(\frac{v_{,y}}{R} \right); \quad \kappa_{xy} = -w_{,xy} + \frac{\delta_1}{2} \left(\frac{v_{,x}}{R} \right) \quad (4)$$

where

$$\delta_1 = \begin{cases} 1 & \text{for Sanders kinematic relations} \\ 0 & \text{for Donnell kinematic relations} \end{cases} \quad (5)$$

II.2 Stress-Strain Relations

The smeared technique (Refs. 16 and 17) is used for the orthogonal stiffeners and the usual lamination theory for the laminate (see Ref. 18). Each lamina is assumed to be orthotropic and the directions of orthotropy make an angle θ with respect to the reference axes x and y . Note that if the orthotropic axis are denoted by "1" and "2", θ is the angle between axes "1" and x , measured counterclockwise from the x -axis.

The stress-strain relations for each lamina are transformed to the xy -axes (18). Moreover, the stress-strain relations for the closely spaced orthogonal and eccentric stiffeners are written on the basis of the assumptions (see Ref. 16) that (i) the stiffeners do not carry shear but only normal stresses, (ii) the stiffeners are torsionally weak and (iii) the stiffener-laminate connection is monolithic. The stiffener eccentricities are positive if the stiffeners are placed on the outer side of the laminate (in the positive z -direction).

Next, the usual stress and moment resultants are defined and their relations to the reference surface (midsurface of the laminate) strains and changes in curvature and torsion are obtained. These are (in matrix form)

$$\begin{Bmatrix} N_{xx} \\ N_{yy} \\ N_{xy} \\ M_{xx} \\ M_{yy} \\ M_{xy} \end{Bmatrix} = \begin{bmatrix} \bar{A}_{11} & \bar{A}_{12} & \bar{A}_{13} & \bar{B}_{11} & \bar{B}_{12} & \bar{B}_{13} \\ \bar{A}_{12} & \bar{A}_{22} & \bar{A}_{23} & \bar{B}_{12} & \bar{B}_{22} & \bar{B}_{23} \\ \bar{A}_{13} & \bar{A}_{23} & \bar{A}_{33} & \bar{B}_{13} & \bar{B}_{23} & \bar{B}_{33} \\ \bar{B}_{11} & \bar{B}_{12} & \bar{B}_{13} & \bar{D}_{11} & \bar{D}_{12} & \bar{D}_{13} \\ \bar{B}_{12} & \bar{B}_{22} & \bar{B}_{23} & \bar{D}_{12} & \bar{D}_{22} & \bar{D}_{23} \\ \bar{B}_{13} & \bar{B}_{23} & \bar{B}_{33} & \bar{D}_{13} & \bar{D}_{23} & \bar{D}_{33} \end{bmatrix} \begin{Bmatrix} \epsilon_{xx}^0 \\ \epsilon_{yy}^0 \\ \gamma_{xy}^0 \\ \kappa_{xx} \\ \kappa_{yy} \\ 2\kappa_{xy} \end{Bmatrix} \quad (6)$$

where

$$[\bar{A}_{ij}] = [A_{ij}] + \begin{bmatrix} \frac{E_x A_x}{l_x} & 0 & 0 \\ 0 & \frac{E_y A_y}{l_y} & 0 \\ 0 & 0 & 0 \end{bmatrix} \quad (7)$$

$$[\bar{B}_{ij}] = [B_{ij}] + \begin{bmatrix} E_x A_x e_x / l_x & 0 & 0 \\ 0 & E_y A_y e_y / l_y & 0 \\ 0 & 0 & 0 \end{bmatrix} \quad (8)$$

$$[\bar{D}_{ij}] = [D_{ij}] + \begin{bmatrix} E_x (I_{xc} + e_x^2 A_x) / l_x & 0 & 0 \\ 0 & E_y (I_{yc} + e_y^2 A_y) / l_y & 0 \\ 0 & 0 & 0 \end{bmatrix} \quad (9)$$

and A_{ij} , B_{ij} and D_{ij} are the usual stiffnesses employed in lamination theory (18). Furthermore, E_x and E_y are Young's moduli for the stringer and ring material, A_x and A_y stiffener cross sectional areas, l_x and l_y stiffener spacings, e_x and e_y stiffener eccentricities, and I_{xc} and I_{yc} second moment of stiffener areas about centroidal axes.

II.3 Equilibrium Equations and Boundary Conditions

The governing equations are derived for an orthogonally and eccentrically stiffened, laminated, imperfect, thin, circular cylindrical shell, subjected to eccentric in-plane loads and uniform external constant-directional pressure. This is done in order to have a set of equations, which can easily be specialized to and accommodate the following constructions and geometries: perfect or imperfect metallic (isotropic) with or without stiffening; and laminates of symmetric, antisymmetric or completely asymmetric lamina stacking. The nonlinear field equations (equilibrium) and related boundary conditions are derived from the principle of the stationary value of the total potential. These equations are:

$$N_{xx,x} + N_{xy,y} = 0$$

$$\begin{aligned}
 & N_{xy,x} + N_{yy,y} - \delta_1 \left[\frac{N_{yy}}{R} \left(\frac{v}{R} - w_{,x} - w_{,x}^0 \right) + \frac{N_{xy}}{R} (w_{,x} + w_{,x}^0) + (M_{xy,x} + M_{yy,y})/R \right] = 0 \\
 & [N_{xx}(w_{,x} + w_{,x}^0)]_{,x} + [N_{xy}(w_{,y} + w_{,y}^0)]_{,x} + [N_{xy}(w_{,x} + w_{,x}^0)]_{,y} \\
 & + [N_{yy}(w_{,y} + w_{,y}^0)]_{,y} - \frac{N_{yy}}{R} - \frac{\delta_1}{R} [(N_{xy}v)_{,x} + (N_{yy}v)_{,y}] \\
 & + M_{xx,x} + 2M_{xy,xy} + M_{yy,yy} + q = 0
 \end{aligned} \tag{10}$$

The boundary conditions at $x = 0$ and L are either natural (force and moments prescribed) or kinematic

Either

$$N_{xx} = -\bar{N}_{xx}$$

$$N_{xy} + \delta_1 M_{xy}/R = \bar{N}_{xy} + \delta_1 \bar{M}_{xy}/R$$

$$N_{xx}(w_{,x} + w_{,x}^0) + N_{xy}(w_{,y} + w_{,y}^0 - \delta_1 \frac{v}{R})$$

$$+ M_{xx,x} + 2M_{xy,y} = \bar{Q}_x + \bar{M}_{xy,y}$$

$$M_{xx} = \bar{M}_{xx}$$

Or

$$u = 0$$

$$v = 0$$

$$w = 0$$

$$w_{,x} = 0$$

(11)

Note that the "bar" quantities denote applied forces and moments.

II.4 A Solution Methodology

The solution procedure consists of several steps, which are outlined herein with brevity (for details see Ref. 15). These steps are:

(1) A separated form is assumed for the three dependent variables $u(x,y)$, $v(x,y)$ and $w(x,y)$ [displacement components].

$$\begin{aligned} u(x,y) &= \sum_{i=0}^k \left[u_{1i}(x) \cos \frac{\ln y}{R} + u_{2i}(x) \sin \frac{\ln y}{R} \right] \\ v(x,y) &= \sum_{i=0}^k \left[v_{1i}(x) \cos \frac{\ln y}{R} + v_{2i}(x) \sin \frac{\ln y}{R} \right] \\ w(x,y) &= \sum_{i=0}^k \left[w_{1i}(x) \cos \frac{\ln y}{R} + w_{2i}(x) \sin \frac{\ln y}{R} \right] \end{aligned} \quad (12)$$

Note that since $\sin \frac{(0) \ln y}{R} = 0$ the functions $u_{20}(x)$, $v_{20}(x)$, and $w_{20}(x)$ do not enter into the solution scheme, and thus the number of independent and unknown functions of position x is $(6k + 3)$.

The known imperfection $w^0(x,y)$ can also be expressed in a form similar to $w(x,y)$. In this case $w^0_{1i}(x)$ and $w^0_{2i}(x)$ are known (taken as known) functions of position.

(2) The expressions for the displacement components are substituted into the kinematic relations, Eqs. (2) and (4). Because of the nonlinearity of the in-plane strain-displacement equations, this substitution yields double summations for the trigonometric functions. These double summations involve products of sines and cosines in all four possible combinations (sine - sine, cosine - cosine, sine-cosine and cosine - sine). Use of trigonometric identities involving products changes the double summation to single summation of either sine or cosine terms but with twice as many terms.

Through this step, all strain components (stretching and bending) can be expressed in terms of sines and cosines of iny/R . Some of the sums go from $i = 0$ to $i = k$ and some from $i = 0$ to $i = 2k$. Note that the coefficients of the sine and cosine terms involve linear and nonlinear combinations of the $(6k + 3)$ dependent functions, u_{1i} , u_{2i} , v_{1i} , v_{2i} , w_{1i} and w_{2i} .

(3) The above separated expressions for the in-plane strains, and changes in curvature and torsion are then substituted into the constitutive equations, Eqs. (6). Since these equations relate the stress and moment resultants to the stretching (ϵ_{ij} 's) and bending (κ_{ij} 's) strains in a linear manner, then use of Eqs. (6) yields single sums of sines and cosines of iny/R , similar to those for strains.

(4) Once steps (2) and (3) are completed, the obtained separated expressions for the stress and moment resultants, along with the assumed expressions for the displacement components (u , v and w) are substituted into the equilibrium equations, Eqs. (10).

Note that some of the stress resultants are multiplied by either some displacement components or their gradients. Because of this one obtains products of sums (of sines and cosines) and some sums go from $i = 0$ to $i = k$ (for the N_{ij} 's). Using a procedure similar to the one outlined in step (2), these products of sums are changed to a single sum and the highest upper limit of the summation is $3k$ (the single sums go from $i = 0$ to $i = 3k$). The boundary conditions, Eqs. (11) can also be expressed in term of the dependent variables, following the above procedure.

(5) The Galerkin procedure is then employed, in the circumferential direction. The vanishing of the Galerkin integrals leads to $(6k + 3)$ unknown functions of position x , $u_{1i}(x)$, $v_{1i}(x)$, $w_{1i}(x)$ for $i = 0, 1, 2 \dots k$, and $u_{2i}(x)$, $v_{2i}(x)$ and $w_{2i}(x)$ for $i = 1, 2, \dots k$.

(6) Next, the generalized Newton's method (19, 17), applicable to differential equations, is used to reduce the nonlinear field equations and boundary conditions to a sequence of linearized systems. The linearized iteration equations are derived based on the conjecture that the solution to the nonlinear set can be achieved by small corrections to an approximate solution. The small corrections or the values of the variables at the $(m + 1)$ th step, in terms of the values at the closely spaced m th state, can be obtained by solving the linearized differential equations. The linearization of a typically nonlinear term (product of X and Y), in the differential equations, is shown below.

$$\begin{aligned}
 X^{m+1} Y^{m+1} &= (X^m + dX^m)(Y^m + dY^m) \\
 &= X^m Y^m + X^m dY^m + Y^m dX^m + dX^m dY^m + X^m Y^m - X^m Y^m \\
 &= X^m (Y^m + dY^m) + Y^m (X^m + dX^m) - X^m Y^m \\
 &= X^m Y^{m+1} + X^{m+1} Y^m - X^m Y^m
 \end{aligned} \tag{13}$$

(7) The order of the linearized differential equations is reduced from four to two by a simple transformation. If the vector of all the unknowns is denoted by $[x]$ (in matrix form) then

$$\{x\} = (u_{1i}^{m+1}, u_{2i}^{m+1}, v_{1i}^{m+1}, v_{2i}^{m+1}, w_{1i}^{m+1}, w_{2i}^{m+1})^T \tag{14}$$

For convenience the number of unknowns is taken as $(6k + 6)$ subject to the constraint

$$u_{20} = v_{20} = w_{20} = 0 \tag{15}$$

The iteration equations can be written in matrix form as

$$[R4]\{x, x_{xx}\} + [R3]\{x, x_{xx}\} + [R2]\{x, x_{xx}\} + [R1]\{x, x\} + [R0]\{x\} = \{g\} \quad (16)$$

By introducing the transformation

$$\{\eta\} = \{x, x_{xx}\} \quad (17)$$

only in connection with the third and fourth derivatives, the iteration equations, Eqs. (16), become

$$[R]\begin{Bmatrix} \{x, x_{xx}\} \\ \{\eta, x_{xx}\} \end{Bmatrix} + [S]\begin{Bmatrix} \{x, x_{xx}\} \\ \{\eta, x_{xx}\} \end{Bmatrix} + [T]\begin{Bmatrix} \{x\} \\ \{\eta\} \end{Bmatrix} = \{G\} \quad (18)$$

where $[R]$, $[S]$, and $[T]$ are $12(k+1)$ by $12(k+1)$ square matrices, with elements involving values of the variables at the m th step [see Eq. (14)] plus other known parameters. $\{G\}$ is a $12(k+1)$ by one matrix with known elements.

Moreover, the boundary terms are also put in matrix form

$$[DB]\begin{Bmatrix} \{x, x_{xx}\} \\ \{\eta, x_{xx}\} \end{Bmatrix} + [DC]\begin{Bmatrix} \{x\} \\ \{\eta\} \end{Bmatrix} = \{BG\} \quad (19)$$

The details can be found in Ref. 15.

(8) The linearized iteration equations, Eqs. (18) are next cast into finite difference form by employing the usual central difference formula. At each end of the cylindrical shell (boundaries $x = 0$ and $x = L$) one fictitious point is used. The required additional equations are provided by the boundary terms, Eqs. (19), and some auxiliary equations, which are also cast in finite difference form.

(9) Finally, the total potential is expressed in terms of the dependent functions and, at each level of the applied loading, its value is computed by numerical integration.

In closing, a computer program has been written to compute the response of the shell at each level of the applied loading. Initially, at a low value of the loading, the solution is estimated through the use of the linear axisymmetric equations. Then, the iteration equations are employed, and by step increasing the loading the complete response (up to the limit point) (20) is obtained.

Several results are obtained by employing this formulation (u, v, w) and are discussed, in detail, in the next chapter.

CHAPTER III

RESULTS AND DISCUSSION; U,V,W - FORMULATION

Numerical results are generated for the u,v,w - formulation, by employing two different digital computers: (a) the interactive computer IBM 43/31 at the Technion Computer Center and (b) the VAX 11/780 of the GTICES (Georgia Tech integrated Computer Engineering System) Systems Laboratory of the School of Civil Engineering.

III.1 Description of Structural Geometry.

Three basic configurations are used in generating results. They consist of an isotropic cylinder, an orthotropic one and a laminated one. All configurations are imperfect, and the imperfection shape is either symmetric or (virtually) axisymmetric. The laminated geometry is the one employed in (21). The properties for each configuration are given separately.

Isotropic Geometry

The isotropic geometry consists of a thin imperfect cylindrical shell with the following dimensions and properties

$$E = 7.24 \times 10^7 \text{ kN/m}^2 (10.5 \times 10^6 \text{ psi}); \nu = 0.30$$

$$R = 10.16 \text{ cm (4 in.)}; 1 \leq L/R \leq 10;$$

$$188.7 \leq R/h \leq 1000.0$$

As seen from the data above, the cylinder length, L, and the shell thickness, h, are varied in order to cover the range of practical interest.

Orthotropic Geometry

The properties of the orthotropic configuration are (given in terms of axes "1" and "2").

$$E_{11} = 2.069 \times 10^8 \text{ kN/m}^2 \text{ (} 30 \times 10^6 \text{ psi)} ; \nu_{12} = 0.21$$

$$E_{22} = 0.1862 \times 10^8 \text{ kN/m}^2 \text{ (} 2.7 \times 10^6 \text{ psi)} ; G_{12} = 0.0448 \times 10^8 \text{ kN/m}^2 \text{ (} 0.65 \times 10^6 \text{ psi)}$$

$$h = 0.05385 \text{ cm (} 0.0212 \text{ in.)} ; R = 10.16 \text{ cm (} 4 \text{ in.) or } 19.05 \text{ cm (} 7.5 \text{ in.)}$$

$$\text{and } 1 \leq L/R \leq 10.$$

If θ is the angle between the orthotropic axis "1" and the reference axis x, both 0° and 90° configurations are employed, herein.

Laminated Geometry

For the laminated geometry, a four-ply laminate is employed. The orthotropic lamina properties are the same as those given for the orthotropic geometry. The total thickness of the laminate and that of each ply are

$$h_{\text{tot}} = 0.05385 \text{ cm. (} 0.0212 \text{ in.) and}$$

$$h_k - h_{k-1} = 0.013462 \text{ cm. (} 0.0053 \text{ in.)}$$

Furthermore, $R = 19.05 \text{ cm (} 7.5 \text{ in.)}$ and

$$L/R = 2, 5, 10.$$

The stacking sequence is

$$I - 1: - 45^\circ / +45^\circ / +45^\circ / -45^\circ$$

where the first number denotes the orientation of the outermost ply with respect to the x-axis, and the last of the innermost. Note that I-1 is a symmetric geometry (with respect to the reference surface - midsurface).

Imperfection Shapes

Two imperfection shapes are used in the study, one which is symmetric and one which is virtually axisymmetric.

$$\text{symmetric: } w^0(x,y) = \xi h \sin \frac{\pi x}{L} \cos \frac{\pi y}{R} \quad (20)$$

$$\text{axisymmetric: } w^0(x,y) = \xi h \left(\cos \frac{2\pi x}{L} - 0.1 \sin \frac{\pi x}{L} \cos \frac{\pi y}{R} \right) \quad (21)$$

where ξ is a measure of the imperfection amplitude. Note that for the symmetric imperfection $\xi = w_{\max}^0/h$, while for the (almost) axisymmetric one, $\xi = w_{\max}^0/1.1h$.

III.2 Numerical Results

For all geometries considered, results are obtained for classical simply supported (SS-3) boundary conditions, Eqs. (22), and zero load eccentricity. The load case considered is uniform axial compression. The primary emphasis in the numerical studies is to establish which (design) parameters influence the accuracy of the Donnell-type of shell approximation and establish the range of these parameters for which the accuracy is acceptable (by comparison to the Sanders-type approximation).

$$\begin{aligned} N_{xx}(0,y) &= -\bar{N}_{xx} ; v(0,y) = w(0,y) = M_{xx}(0,y) = 0 \\ N_{xx}(L,y) &= -\bar{N}_{xx} ; v(L,y) = w(L,y) = M_{xx}(L,y) = 0 \end{aligned} \quad (22)$$

Numerical results were generated by employing two different computers:

- (a) the interactive computer IBM 43/31 at the Technion (Israel Institute of Technology) Computer Center and b) the VAX 11/780 of the GTICES (Georgia Tech Integrated Computer Engineering System) Systems Laboratory of the School of Civil Engineering.

The results for each geometry are presented and discussed separately.

Isotropic Geometry

The results are presented (in part) graphically on Fig. 3 and in tabular form on Table 1. On Table 1, the geometry, as well as the computed critical loads ($N_{xxCQ} = 0.606 Eh^2/R$ and N_{xx}^l : limit point loads), the corresponding wave number, n , and the imperfection amplitude parameter ξ are presented.

One observation is that the discrepancy between critical loads obtained from the two different shell theory approximations (Sanders and Donnell), is primarily affected by L/R and there is a small effect of R/h . Note that as L/R increases the difference between the two results increases. Moreover, for the same L/R there is a small R/h effect. As R/h decreases the difference increases. The combined effect is shown on Fig. 3 by plotting ρ versus the square root of the Batdorf curvature parameter, Z , defined by

$$Z = \frac{L^2}{Rh} \sqrt{1 - \nu^2}$$

Furthermore, the obtained results substantiate the contention (2) that the Donnell approximation is dependent on the wave number, n . Clearly, from Table 1, if $n > 4$ the two theories yield the same critical load (within one percent), but for $n \leq 4$ the computed difference can be as large as ten percent.

Finally, from Fig. 3, one can see that the imperfection sensitivity decreases with increasing values for the curvature parameter. This is so because, for the same value of the imperfection amplitude parameter, ξ , the

TABLE 1. CRITICAL LOADS (ISOTROPIC GEOMETRY) ;
SS-3; AXISYMMETRIC IMPERFECTION

Case	R cm(in.)	L/R	R/h	$\bar{N}_{xx} c l$ kN/cm (lbs/in.)	$\rho = \frac{-l}{\bar{N}_{xx} c l}$		n: wave No.		ξ Imp. Ampl.	Z
					Sanders	Donnell	Sanders	Donnell		
1	10.16(4)	1	1000.0	4.457 (25.45)	0.652	0.652	13	13	0.5	30.
2	10.16(4)	1	1000.0	4.457 (25.45)	0.446	0.446	13	13	1.0	30.
3	10.16(4)	1	250.0	71.319 (407.23)	0.246	0.248	8	8	1.0	15.
4	10.16(4)	5	250.0	71.319 (407.23)	0.703	0.719	4	4	1.0	77.
5	10.16(4)	10	250.0	71.319 (407.23)	0.790	0.831	3	3	1.0	154.
6	10.16(4)	2	188.7	125.208 (714.94)	0.395	0.396	6	6	1.0	26.
7	10.16(4)	5	188.7	125.208 (714.94)	0.652	0.677	4	4	1.0	67.
8	10.16(4)	10	188.7	125.208 (714.94)	0.753	0.830	3	3	1.0	134.2

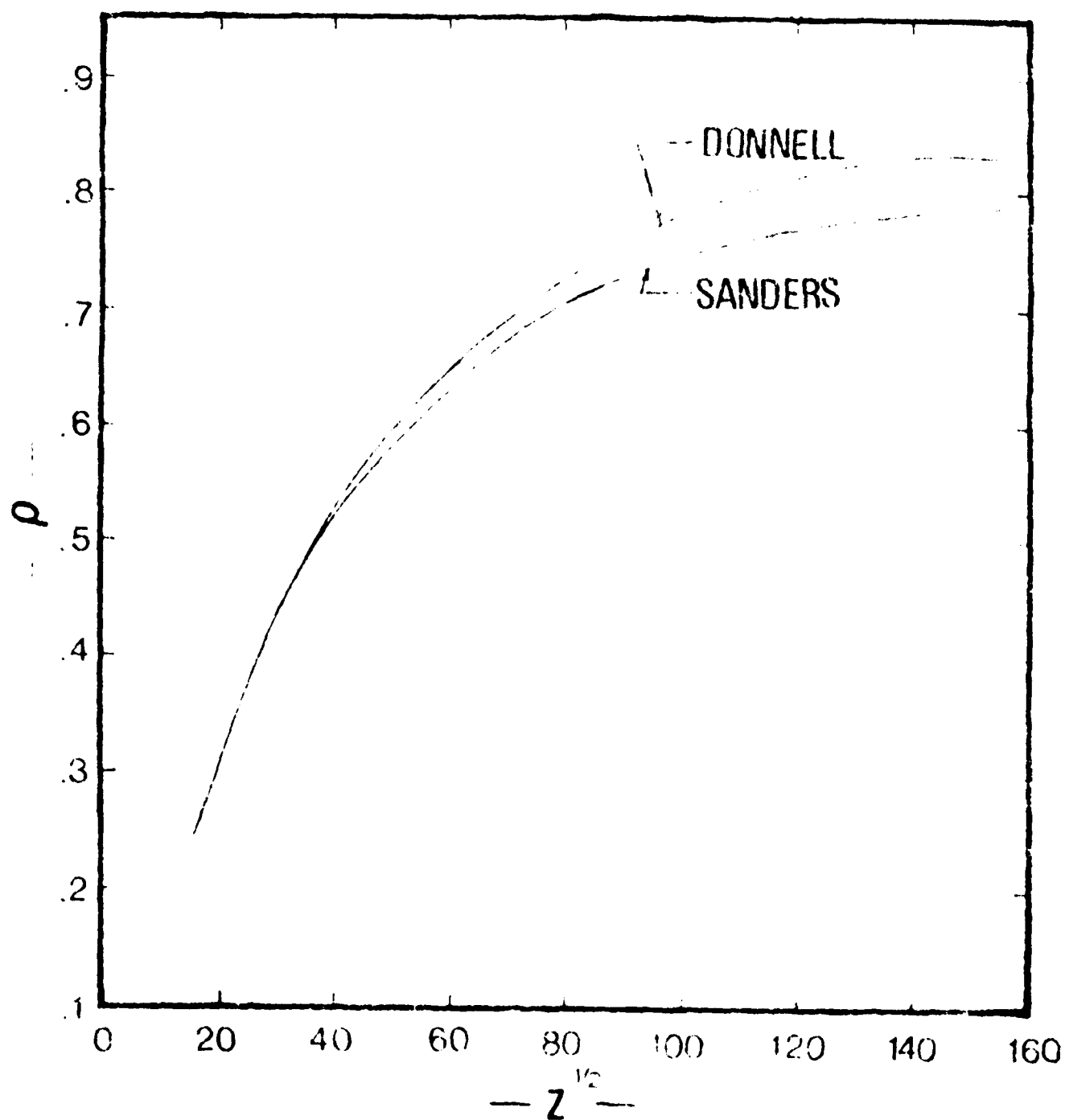


Fig. 3. Load Parameter, ρ ($= \bar{N}_{xx}^l / \bar{N}_{xx_{cl}}$) vs. Curvature

Parameter (Isotropic Geometry; SS-3, Axisym. Imp.)

computed limit point value approaches the classical value (ρ increases) as Z increases. Please note that the curves on Fig. 3 are drawn from points corresponding to different L/R and R/h values.

In closing, it is worth mentioning that Hoff and Soong (22) plotted similar results for perfect isotropic cylinders (using linear theory), but for the SS-1 boundary condition, i.e.,

$$\text{at } x = 0, L: N_{xx} = -\bar{N}_{xx}, N_{xy} = 0, w = 0 \text{ and } M_{xx} = 0 \quad (23)$$

Their (22) results show that the two approximations yield very close critical loads (linear theory eigen-values).

Orthotropic Geometry

The orthotropic geometries and their properties are described in the previous section. The numerical results are presented in tabular form, Tables 2 and 3, and graphically in Figs. 4 and 5.

Table 2 contains results for various orthotropic configurations with a virtually axisymmetric imperfection and $\xi = 1$ [see Eq. (21)]. The first column denotes the angle that the strong direction makes with the x -axis. The next three columns describe the geometry. The classical value is estimated from the data of Ref. 23 (see Fig. 10c of this reference; $D_k/D\theta$ is assumed to be one). The value of \bar{N}_{xx} should only be considered an approximation used as a weighting function. This classical value, which is based on a linear eigenvalue approach is independent of the R/L ratio (this is also true for isotropic geometries). The data of Table 2 are plotted on Fig. 4. Through the plots one may assess better the effect of certain parameters. Fig. 4 shows plots of ρ (the ratio of the limit point load to the classical load) versus $\sqrt{L^2/Rh}$, which is similar to the Batdorf

curvature parameter for isotropic construction, for both shell approximations and separately for the two angles that the strong direction makes with the x-axis. It is seen from Fig. 4 that the behavior is similar to that of the isotropic geometry (see Fig. 3), but it is more pronounced for the 0° -curves than it is for the 90° -curves. In other words, when the strong axis is in the x-direction, the Donnell approximation is accurate (within 6%) even for large values of the curvature parameter (for $L^2/Rh \leq 20,000$). For the 90° -curves the trend is the same, but the Donnell approximation yields less accurate results even for small values of the curvature parameter. Note that, as in the isotropic case, the effect of L/R is the predominant one, while the effect of R/h is negligibly small. Moreover, note that part of the effect due to the construction (orthotropic) is buried in the weighting parameter \bar{N}_{xxcl} , because \bar{N}_{xxcl} is dependent upon the E_{xx}/E_{yy} ratio. Finally, it is worth mentioning that, regardless of the approximation (Sanders or Donnell), when the strong direction is along the x-axis the configuration is more sensitive to the initial imperfection than when the strong direction is in the hoop direction (ρ for 0° is smaller than ρ for 90° , everything else being equal).

Similar results are presented on Table 3 and Fig. 5, with the same observations. The main difference here is that the imperfection is symmetric and the R/h ratio is constant. It is stressed again that the classical critical load is approximate in nature (taken from data of Ref. 23) and thus the critical load parameter ρ -values should be considered as qualitative rather than quantitative.

TABLE 2: CRITICAL CONDITIONS FOR ORTHOTROPIC GEOMETRIES

$$[w^0 = h \left(\cos \frac{2\pi x}{L} - 0.1 \sin \frac{\pi x}{L} \cos \frac{\pi y}{R} \right)]$$

θ , Angle of Strong Direction	R/h	L/R	$(L^2/Rh)^{1/2}$	\bar{N}_{xx}^l lbs/in.		$\bar{N}_{xx}^* c_l$ lbs/in	$\rho = \bar{N}_{xx}^l / \bar{N}_{xx}^* c_l$	
				Sanders (Wave No.)	Donnell (Wave No.)		Sanders	Donnell
0°	188.7	2	27.5	92(7)	92(7)	487	0.189	0.189
0°	↓	5	68.7	222(5)	229(5)	↓	0.456	0.470
0°	↓	10	137.4	265(4)	283(5)	↓	0.544	0.581
90°	↓	2	27.5	230(10)	260(11)	481	0.478	0.541
90°	↓	1	13.7	157(6)	159(6)	↓	0.326	0.331
0°	353.8	2	37.6	69(8)	69(8)	270	0.256	0.256
0°	↓	5	94.0	132(6)	-	↓	0.489	-
90°	↓	2	37.6	127(7)	144(6)	262	0.485	0.550
90°	↓	1	18.8	108(7)	111(7)	↓	0.412	0.424

*Values estimated (calculated) from data of Ref. 23.

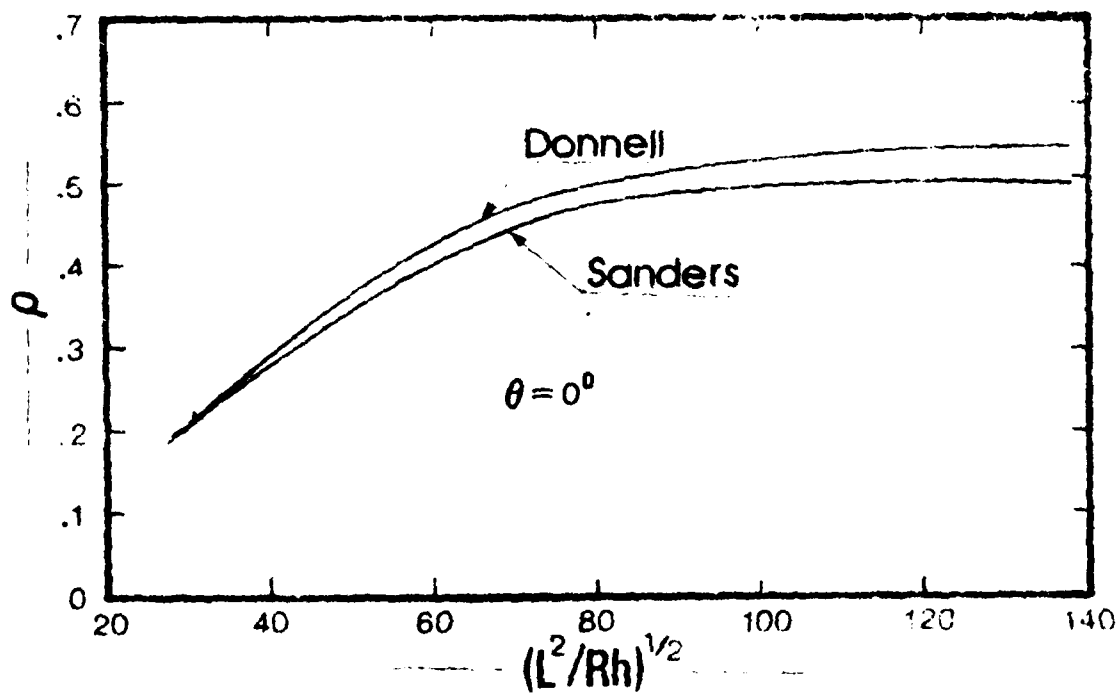
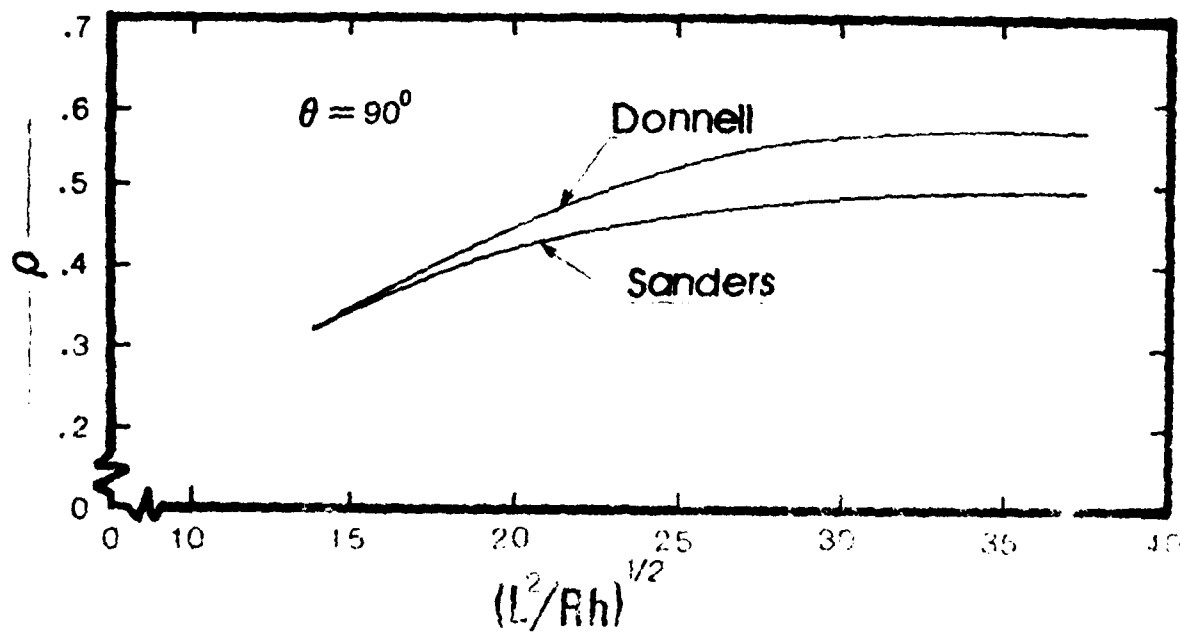



Fig. 4. Load Parameter ρ ($= \bar{N}_{xx}^l / \bar{N}_{xx_{cl}}$) vs. $(L^2/Rh)^{1/2}$

(Orthotropic Geometry; SS-3; Axisym. Imp.)

TABLE 3. CRITICAL CONDITIONS FOR ORTHOTROPIC GEOMETRIES

$$(w^0 = h \sin \frac{\pi x}{L} \cos \frac{\pi y}{R})$$

θ Angle of Strong Direction	R/h	L/R	$(L^2/RH)^{1/2}$	\bar{N}_{xx}^l in lbs/in.		$\bar{N}_{xx}^*_{cl}$ lbs/in	$\rho = \bar{N}_{xx}^l / \bar{N}_{xx}^*_{cl}$	
				Sanders	Donnell		Sanders	Donnell
				(Wave No.)	(Wave No.)			
0°	353.8	2	37.6	85(9)	85(9)	270	0.315	0.315
0°		5	94.0	125(6)	130(6)	↓	0.463	0.481
0°		10	188.0	155(4)	165(4)	↓	0.574	0.611
90°		2	37.6	145(5)	152(5)	262	0.553	0.580
90°		5	94.0	195(4)	215(4)	↓	0.744	0.821
90°		10	188.0	212(3)	271(3)	↓	0.809	1.034

*Values estimated from data of Ref. 23.

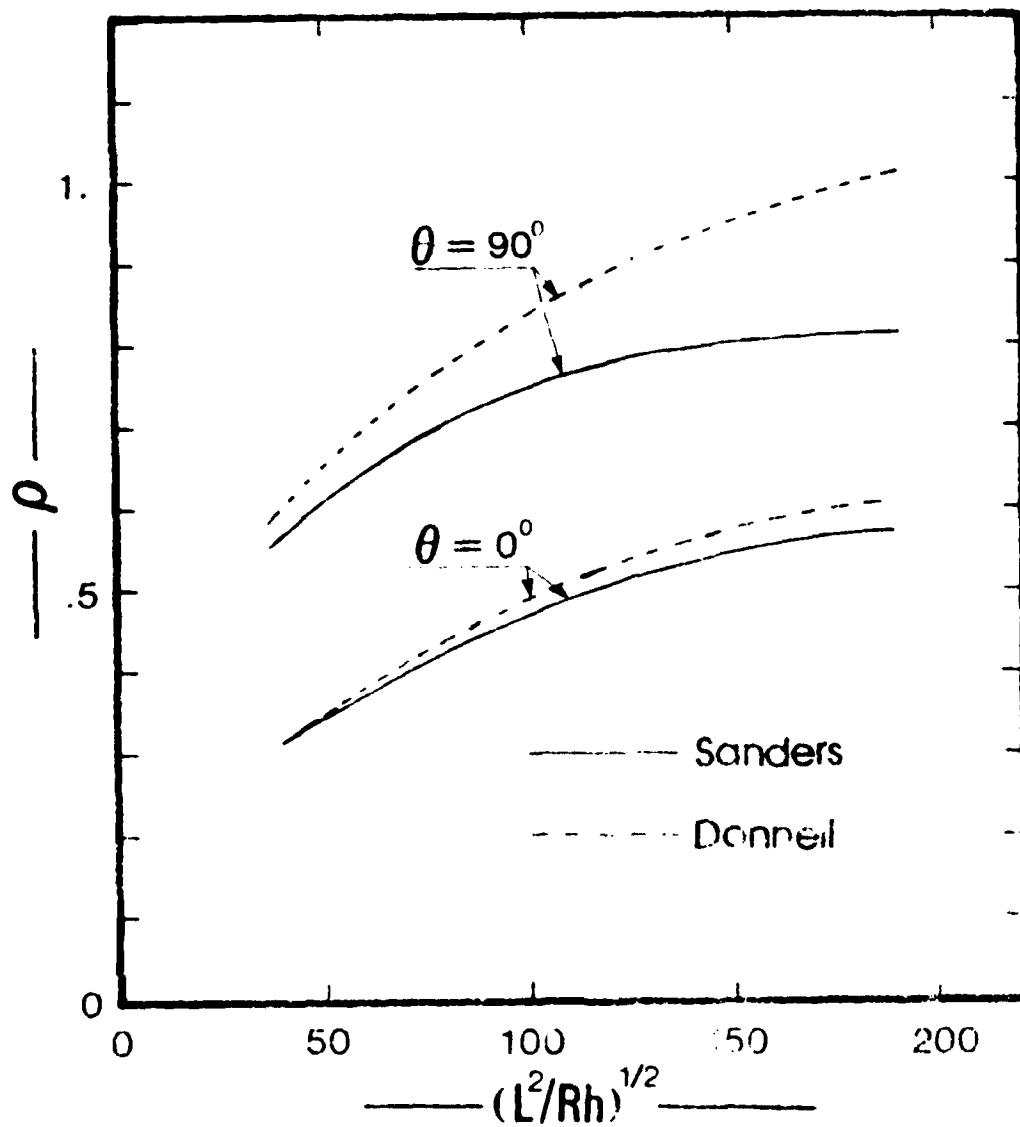


Fig. 5. Load Parameter ρ ($= \bar{N}_{xx}^l / \bar{N}_{xx_{cl}}$) vs. $(L^2/Rh)^{1/2}$
(Orthotropic Geometry; SS-3; Sym. Imp.)

Laminated Geometry

For this geometry, the symmetric imperfection shape, Eq. (20), and the geometric and material properties are presented in a previous article.

This geometry is taken from (21) in which experimental results are reported for $L/R = 2$. Note also that because of the stacking (symmetric and $\pm 45^\circ$), the resulting configuration has $B_{ij} = 0$, and in-plane (A_{ij}) and bending (D_{ij}) stiffness parameters that are similar to an isotropic configuration.

For this geometry results are generated for several ξ -values (imperfection sensitivity study) and three values of L/R (2,5,10).

The results are presented in tabular (Table 4) and graphical form (Fig. 6).

As seen from Table 4, the trend is the same as for the isotropic geometry. For $L/R = 2$ the two shell theory approximations yield the same critical load for all values of the imperfection amplitude parameter, but different for higher values of L/R . Moreover, the wave number for $L/R = 2$ is six, while for $L/R = 5$ is four, and for $L/R = 10$ is three. The similarity in behavior between the isotropic and the laminated geometries is primarily attributed to the fact that for the laminated geometry $B_{ij} = 0$, $A_{11} = A_{22}$ and $D_{11} = D_{22}$, which makes the elements of the A_{ij} and D_{ij} matrices be similar to the elements of an isotropic configuration.

One important difference is that the critical load for the corresponding perfect laminated geometry appears to be heavily dependent upon the value of L/R (observation made by extrapolation of ξ curves in Fig. 6). Finally, it is seen from Fig. 6 that the laminated geometry, regardless of the shell theory, becomes more sensitive to initial geometric

imperfections as L/R increases. For $L/R \pm 2$ the curve is rather flat but for $L/R = 10$, the curve drops rapidly. These observations are made on the basis of the generated results (limited), and they should not be generalized.

TABLE 4. CRITICAL LOADS (LAMINATED GEOMETRY)

ξ	Critical Load, kN/cm (lbs/in)								
	$L/R = 2$			$L/R = 5$			$L/R = 10$		
	Sanders	n	Donnell	Sanders	n	Donnell	Sanders	n	Donnell
0.5	22.767 (130.00)	6	22.767 (130.00)	25.744 (147.00)	4	26.444 (151.00)	43.783 (250.00)	3	63.047 (360.00)
1.0	20.665 (118.00)	6	21.103 (120.50)	22.767 (130.00)	4	24.518 (140.00)	33.275 (190.00)	3	45.534 (260.00)
2.0	17.368 (98.60)	6	17.391 (99.30)	19.264 (110.30)	4	21.366 (122.00)	26.270 (150.00)	3	35.902 (205.00)

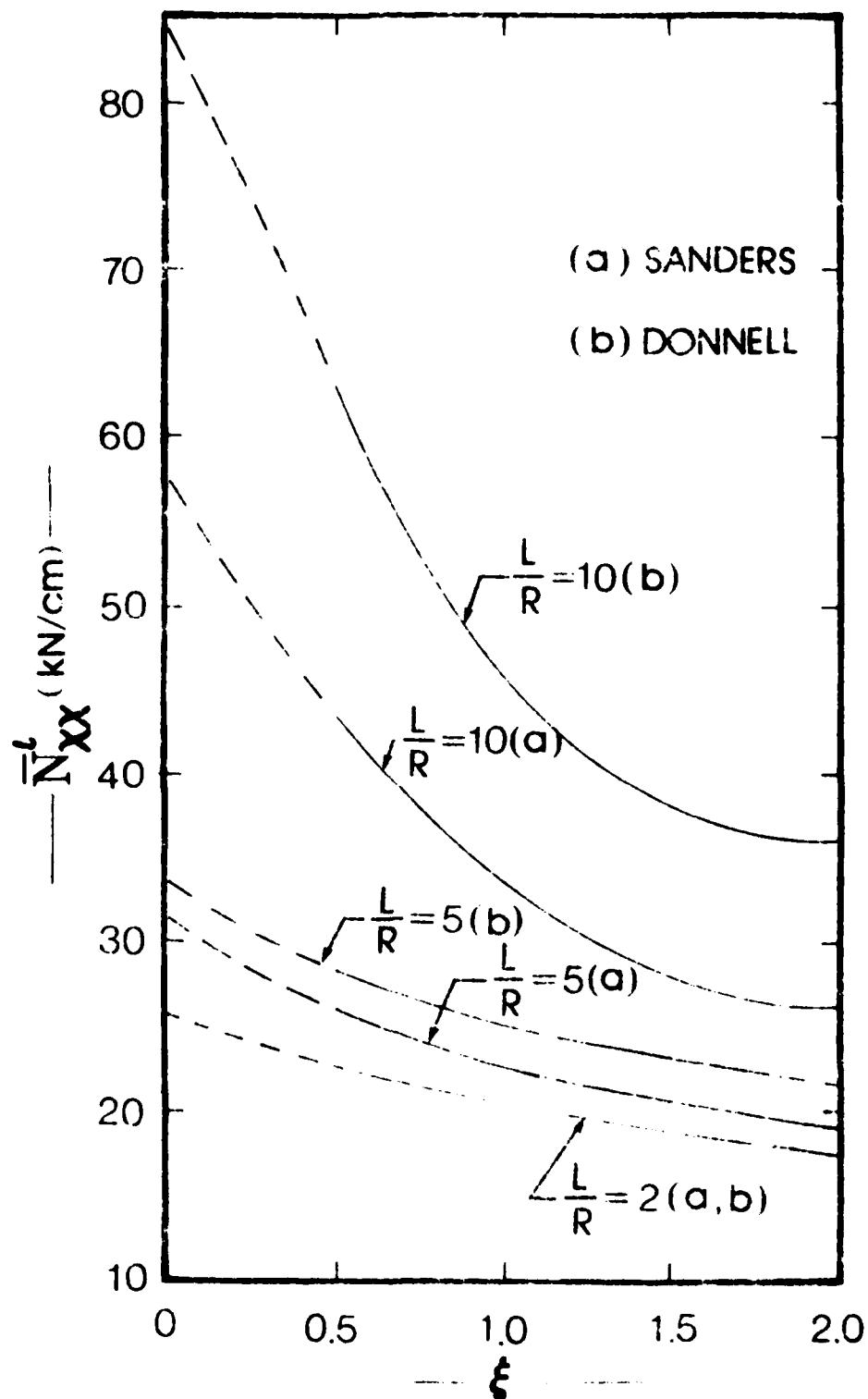


Fig. 6. Critical Loads for the Laminated Geometry
 (SS-3; Symmetric Imp.)

CHAPTER IV

ADDITIONAL RESULTS; w,F - FORMULATION

In addition to the results reported in Chapter III, certain parametric studies were performed by employing the w,F-formulation (Ref. 15). These studies include assessment of imperfection sensitivity and of the effect of lamina stacking on the critical conditions of four-and six-ply laminated cylinders under axial compression and torsion (individually applied). These geometries represent variations of two symmetric geometries reported in Ref. 21. Moreover, the effect of L/R-ratios on critical loads is assessed for the four-ply and the six-ply geometries. In all of these studies the load eccentricity is taken to be zero and the boundaries are simply supported (SS-3). The geometries employed in the parametric studies and the results are next presented, separately.

IV. 1 Description of Geometry

Two basic laminated configurations are used in generating results. They consist of four-ply laminates, I-i, using various stacking sequences, and of six-ply laminates, II-i with different stacking sequences. For both groups five stacking sequences ($i = 1, 2, \dots, 5$) are employed.

First, the common properties of the orthotropic laminae (Boron/Epoxy; AVCO 5505) are:

$$\begin{aligned} E_{11} &= 2.0690 \times 10^8 \text{ kN/m}^2 \text{ (30} \times 10^6 \text{ psi)} \\ E_{22} &= 0.1862 \times 10^8 \text{ kN/m}^2 \text{ (2.7} \times 10^6 \text{ psi)} \\ G_{12} &= 0.0448 \times 10^8 \text{ kN/m}^2 \text{ (0.65} \times 10^6 \text{ psi)} \end{aligned} \quad (24)$$

Furthermore,

$$R = 19.05 \text{ cm (7.5 in.)}$$

and the length, L , is varied so that

$$L/R = 1, 3 \text{ and } 5.$$

The ply thicknesses ($h_k - h_{k-1}$) and the total laminate thickness for each group is:

$$\text{I-i; } h_k - h_{k-1} = 0.013462 \text{ cm (0.0053 in.)} \quad (25a)$$

$$h = 4(h_k - h_{k-1}) = 0.05385 \text{ cm. (0.0212 in.)}$$

$$\text{and II-i; } h_k - h_{k-1} = 0.008975 \text{ cm (0.003533 in.)} \quad (25b)$$

$$h = 6(h_k - h_{k-1}) = 0.05385 \text{ cm (0.0212 in.)}$$

Note that for both groups (I-i and II-i), the radius to thickness ratio is 353.77 ($=R/h$).

For each group the five stacking combinations are denoted by I-i or II-i, $i = 1, 2, \dots, 5$ and they correspond to

$$\text{I-1} = 45^\circ/-45^\circ/-45^\circ/45^\circ; \text{ I-2: } 45^\circ/-45^\circ/45^\circ/-45^\circ; \quad (26a)$$

$$\text{I-3} = -[\text{I-2}]; \text{ I-4: } 90^\circ/60^\circ/30^\circ/0^\circ; \text{ I-5: } 0^\circ/30^\circ/60^\circ/90^\circ$$

$$\text{II-1: } 0^\circ/45^\circ/-45^\circ/-45^\circ/45^\circ/0^\circ$$

$$\text{II-2: } -45^\circ/45^\circ/-45^\circ/45^\circ/-45^\circ/45^\circ/45^\circ$$

$$\text{II-3} = -[\text{II-2}]$$

$$\text{II-4 : } -90^\circ/72^\circ/54^\circ/36^\circ/18^\circ/0^\circ$$

$$\text{II-5 : } 0^\circ/18^\circ/36^\circ/54^\circ./72^\circ/90^\circ$$

(26b)

Where the first number denotes the orientation of the fibers (strong orthotropic direction) of the outermost ply with respect to the x -axis, and the last of the innermost. Note that in the u,v,w -formulation, geometry I-1 (same as in this chapter) is listed as $-45^\circ/45^\circ/45^\circ/-45^\circ$. This is so because the system of reference axes used in the u,v,w -formulation (see Fig. 1) is different from the one employed in the

w,F-formulation (see Ref. 15) [the x-axis is the same as shown on Fig. 1, but the y-and z-axes are opposite from those shown on Fig. 1].

Geometries I-1 and II-1 are symmetric with respect to the midsurface and they are identical to those employed in Ref. 21. Geometries I-2,3 and II-2,3 denote antisymmetric, regular ($h_k - h_{k-1} = \text{constant}$) angle-ply laminates. Finally, geometries, I-4,5 and II-4,5 are completely asymmetric with respect to the midsurface.

Two load cases are considered and for each load case different imperfection shapes are employed. These are:

(a) for uniform axial compression

(a) for geometries I-i ($i = 1, 2 \dots 5$)

$$w^0(x, y) = \frac{1}{2} h \sin \frac{\pi x}{L} \cos \frac{\pi y}{R} \quad (27)$$

(b) for geometries III-i ($i = 1, 2, \dots 5$)

$$w^0(x, y) = \frac{1}{2} h \left(-\cos \frac{2\pi x}{L} + 0.1 \sin \frac{\pi x}{L} \cos \frac{\pi y}{R} \right) \quad (28)$$

Note that the first one, Eq. (27) denotes a symmetric shape, while the second one, Eq. (28), an (almost) axisymmetric shape.

(b) for torsion

(a) for $L/R = 1$

$$\begin{aligned} \text{I-i: } w^0(x, y) = 0.6235383 \frac{1}{2} h \left[\left(\sin \frac{\pi x}{L} - \frac{1}{3} \sin \frac{3\pi x}{L} \right) \cos \frac{\pi y}{R} \right. \\ \left. + \left(\sin \frac{2\pi x}{L} - \frac{1}{2} \sin \frac{4\pi x}{L} \right) \sin \frac{\pi y}{R} \right] \end{aligned} \quad (29a)$$

$$\begin{aligned} \text{II-i: } w^0(x, y) = \frac{1}{2} h \left[-0.583133 \left(\sin \frac{\pi x}{L} - \frac{1}{3} \sin \frac{3\pi x}{L} \right) \cos \frac{\pi y}{R} \right. \\ \left. + 0.647926 \left(\sin \frac{2\pi x}{L} - \frac{1}{2} \sin \frac{4\pi x}{L} \right) \sin \frac{\pi y}{R} \right] \end{aligned} \quad (29b)$$

(b) for $L/R = 2$ and both groups

$$\begin{aligned} w^0(x, y) = \frac{1}{2} h \left[-0.536769 \left(\sin \frac{\pi x}{L} - \frac{1}{3} \sin \frac{3\pi x}{L} \right) \cos \frac{\pi y}{R} \right. \\ \left. + 0.670961 \left(\sin \frac{2\pi x}{L} - \frac{1}{2} \sin \frac{4\pi x}{L} \right) \sin \frac{\pi y}{R} \right] \end{aligned} \quad (3c)$$

(c) for $L/R = 5$ and both groups

$$w^0(x,y) = \frac{2}{3} h \left[-0.417060 \left(\sin \frac{\pi x}{L} - \frac{1}{3} \sin \frac{3\pi x}{L} \right) \cos \frac{\pi y}{R} \right. \\ \left. + 0.694444 \left(\sin \frac{2\pi x}{L} - \frac{1}{2} \sin \frac{4\pi x}{L} \right) \sin \frac{\pi y}{R} \right. \\ \left. + 0.833333 \left(\frac{1}{3} \sin \frac{3\pi x}{L} - \frac{1}{5} \sin \frac{5\pi x}{L} \right) \cos \frac{\pi y}{R} \right] \quad (31)$$

For this load case (torsion), the imperfection shape is taken to be similar to the linear theory buckling mode (see Ref. 15). These shapes, Eqs. (29), (30), and (31), represent some average of the modes of the various configurations (the modes are very similar for all configurations).

IV.2 Discussion of Results

The results for all configurations are presented both graphically and in tabular form. Each group through, is discussed separately.

Table 5 presents critical loads (limit point loads-uniform axial compression) for geometries I-i and three values of L/R (1,2 and 5). The imperfection shape for this group is symmetric, Eq. (27), and the amplitude parameter is varied from a small number up to two ($w^0_{max}/h = \frac{2}{3}$). The values obtained from the w,F -formulation differ slightly from those obtained by the u,v,w -formulation (see Table 4). The difference is not caused by the two different formulations (both based on Donnell equations), but it is attributed to the fact that the load step in the u,v,w -formulation is larger than in the w,F -formulation. This is so, because it is much more expensive (in time and money) to run the program for the former formulation. It is seen from Figs. 7-9 that, for $L/R = 1$ and small values for $\frac{2}{3}$ ($\frac{2}{3} < 0.75$), the weakest configuration corresponds to I-2,3 (regular antisymmetric angle-ply laminate), while the strongest configuration is the

TABLE 5. CRITICAL LOADS; UNIFORM AXIAL
COMPRESSION (I-i GEOMETRIES)

Geometry	ξ	$\frac{-l}{N_{xx}}$ in lbs/in (wave No. at Limit Pt.)		
		L/R = 1	L/R = 2	L/R = 5
I - 1	0.05	-	145.6 (6)	-
	0.10	130.7 (9)	-	153.7 (4)
	0.50	118.9 (9)	136.0 (6)	147.7 (4)
	1.00	104.5 (9)	123.0 (6)	135.9 (4)
	2.00	67.1 (9)	98.3 (6)	121.0 (4)
I - 2,3	0.05	-	138.8 (6)	-
	0.10	126.7 (9)	-	145.3 (4)
	0.50	115.1 (9)	130.0 (6)	140.2 (4)
	1.00	98.6 (9)	118.7 (6)	129.0 (4)
	2.00	61.3 (9)	92.2 (6)	111.4 (4)
I-4	0.01	-	243.1 (8)	-
	0.05	-	232.0 (8)	245.4 (5)
	0.10	189.9 (12)	-	-
	0.50	130.7 (11)	178.0 (8)	211.5 (5)
	1.00	86.8 (11)	137.2 (8)	187.7 (5)
	2.00	46.1 (10)	90.0 (8)	153.4 (5)
I-5	0.05	-	233.3 (8)	292.9 (5)
	0.10	183.3 (11)	-	-
	0.50	146.3 (11)	191.0 (8)	268.3 (5)
	1.00	97.5 (12)	150.0 (8)	239.0 (5)
	2.00	48.0 (11)	109.5 (8)	194.0 (5)

Symmetric Imperfection

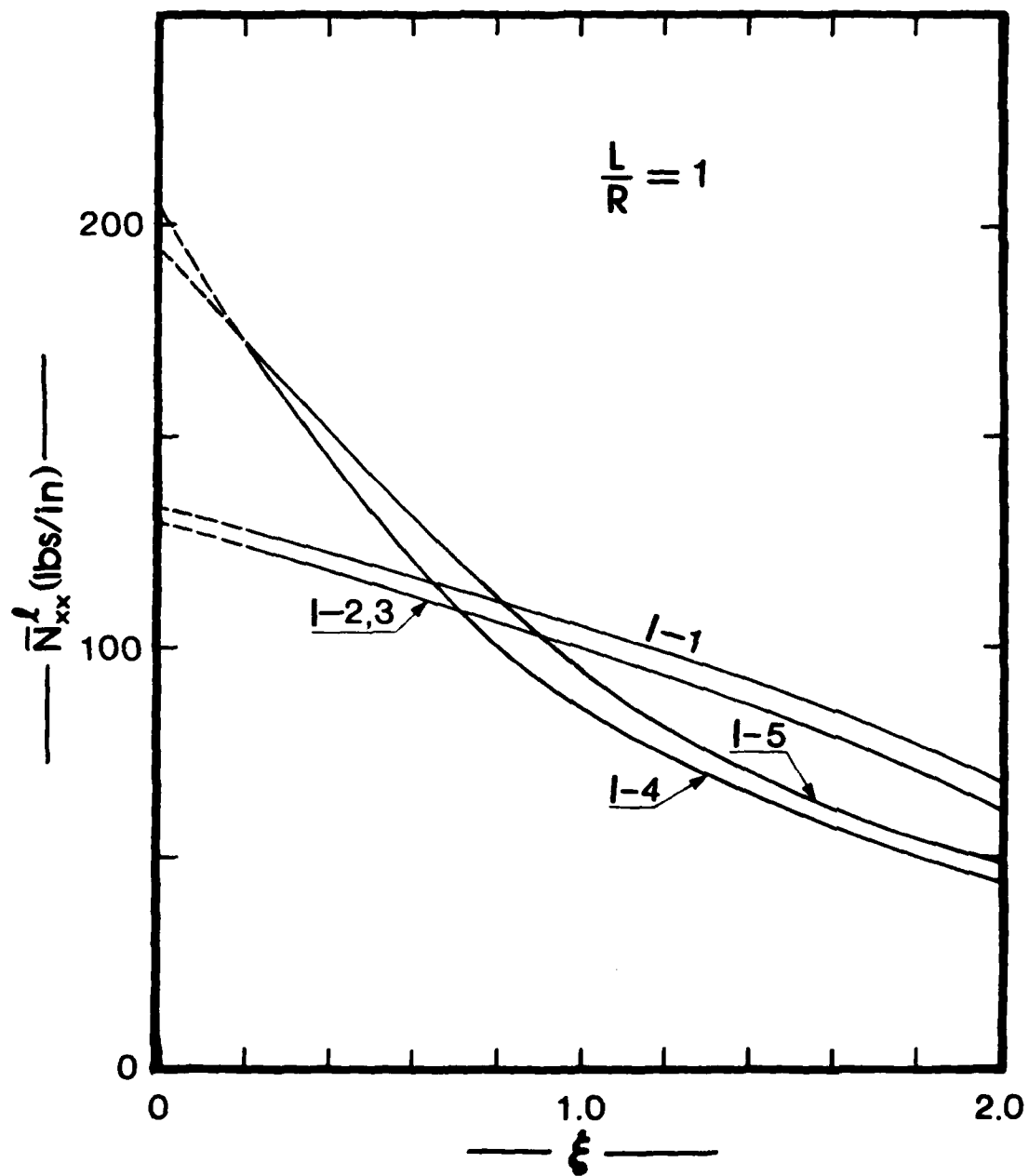


Fig. 7. Critical Conditions for I-i Geometries;
Uniform Axial Compression; $L/R = 1$
(SS-3; Symmetric Imp.)

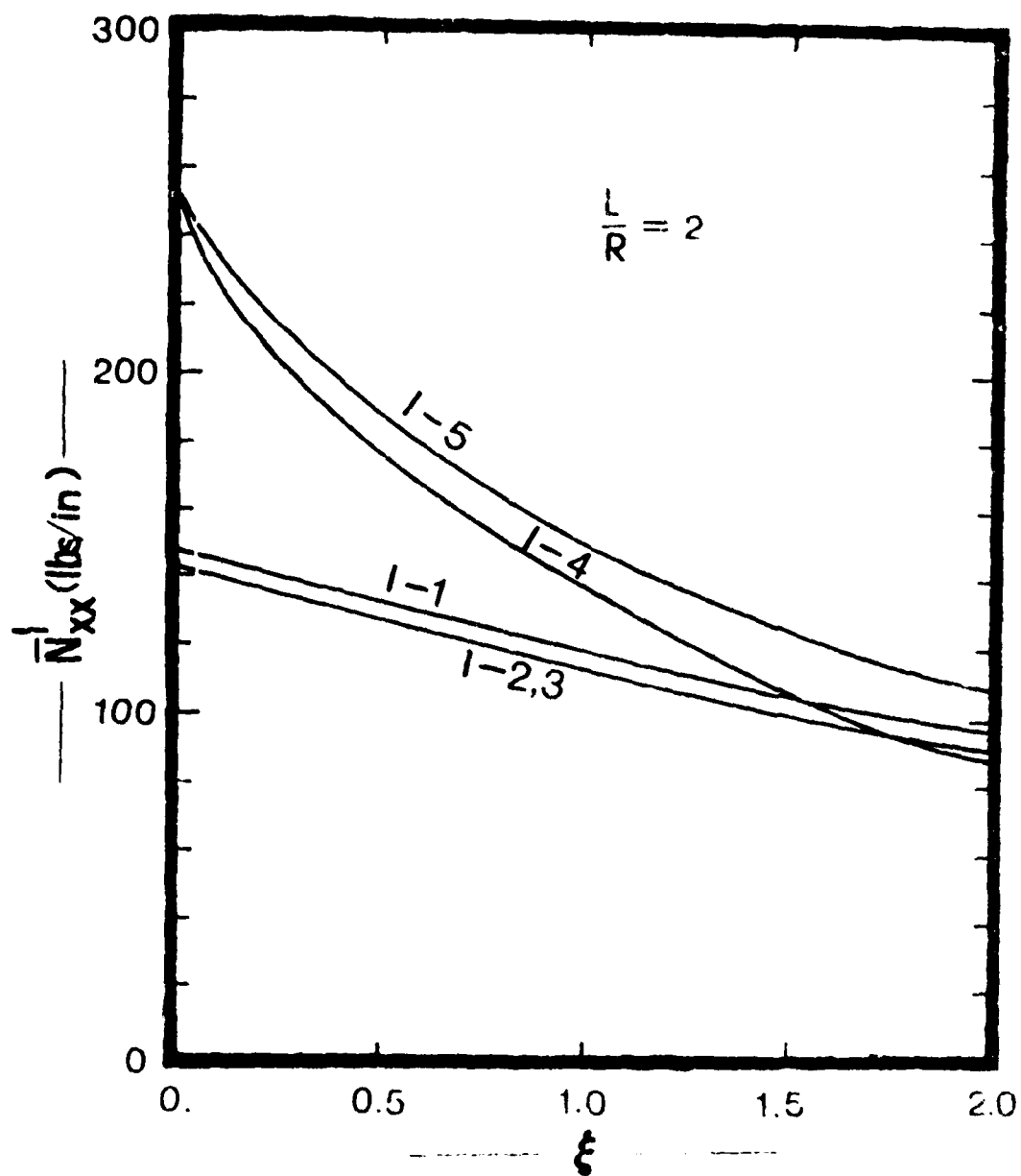


Fig. 8 Critical Conditions for I-1 Geometries;
Uniform Axial Compression; $L/R = 2$
(SS-3; Symmetric Imp.)

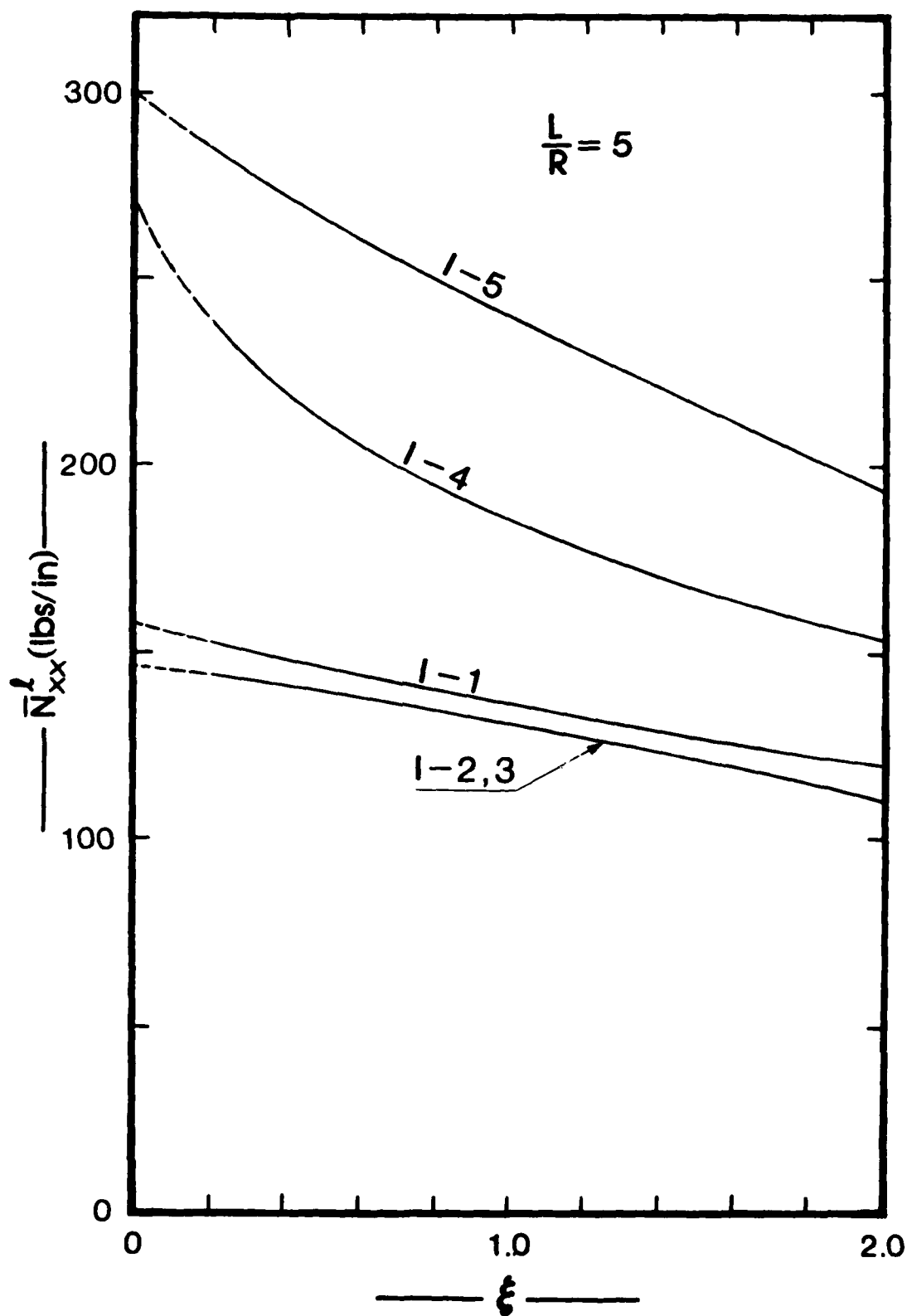


Fig. 9. Critical Conditions for I-1 Geometries;
Uniform Axial Compression; $L/R = 5$
(SS-3; Symmetric Imp.)

asymmetric I-5 (except for a very small range of extremely small ξ - values). But, as L/R increases, I-2,3 yields the weakest configurations for virtually all ξ -values. Moreover, for $L/R > 2$ the order of going from the weakest to the strongest configuration is I-2,3, I-1, I-4 and I-5. Note that asymmetric stacking may be compared to eccentric positioning of the orthogonal stiffeners in metallic shells.

Table 6 presents critical loads (uniform compression) for geometries II-i. The results are similar to those for group I (geometries I-i) but with one exception; geometry II-1 is among the strong configurations, while I-1 is among the weak configurations, especially for higher L/R ratios (see Figs. 10-12 and 7-9). The reason for this is that the II-1 geometry has 0° plies on the outside and inside of the laminate, which increases its stiffness in the axial direction.

The results, for this group, are also presented graphically on Figs. 10-12. Fig. 10 contains results for $L/R = 1$. No results are reported (limit points could not be found) for $\xi > 1.0$. This implies, that for this L/R value and $\xi > 1$ the load-deflection curve does not exhibit limit point instability, but only stable response. For $L/R \geq 2$, the picture changed and limit points are found. Note from the three figures, Figs. 10-12, that as L/R increases the imperfection sensitivity of all configurations decreases (the curves do not fall as sharply as they do for $L/R = 1$).

It is worth noticing that for $L/R \leq 2$, there are many crossings of the curves and it is not easy to identify the strongest or the weakest configuration (which is ξ -dependent). On the other hand, at $L/R = 5$, the strongest configuration is II-5 and the order of going from the strongest to the weakest is, II-5, II-1, II-4, II-2,3. As expected, the $\pm 45^\circ$

TABLE 6. CRITICAL LOADS; UNIFORM AXIAL
COMPRESSION (II-i GEOMETRIES)

Geometry	ξ	\bar{N}_{xx} in lbs/in. (wave No. at Limit Pt)		
		L/R = 1	L/R = 2	L/R = 5
II-1	0.10	231.7 (12)	244.86 (8)	255.6 (5)
	0.50	120.9 (11)	171.3 (8)	219.4 (5)
	1.00	63.4 (10)	112.5 (8)	182.7 (5)
	2.00	-	58.4 (7)	128.2 (5)
II - 2,3	0.10	133.5 (9)	140.5 (6)	150.8 (4)
	0.50	120.7 (9)	134.6 (6)	147.8 (4)
	1.00	87.2 (9)	114.1 (6)	136.2 (4)
	2.00	44.7 (8)	72.6 (6)	111.4 (4)
II - 4	0.10	177.7 (10)	211.3 (8)	227.0 (5)
	0.50	101.7 (10)	157.0 (7)	199.3 (5)
	1.00	57.9 (10)	108.7 (7)	171.0 (5)
	2.00	-	56.8 (7)	128.8 (5)
II-5	0.10	173.5 (11)	199.5	275.0 (5)
	0.50	124.0 (10)	191.3	261.7 (5)
	1.00	66.7 (10)	139.0	227.9 (5)
	2.00		70.4 (7)	168.4 (5)

Axisymmetric Imperfection

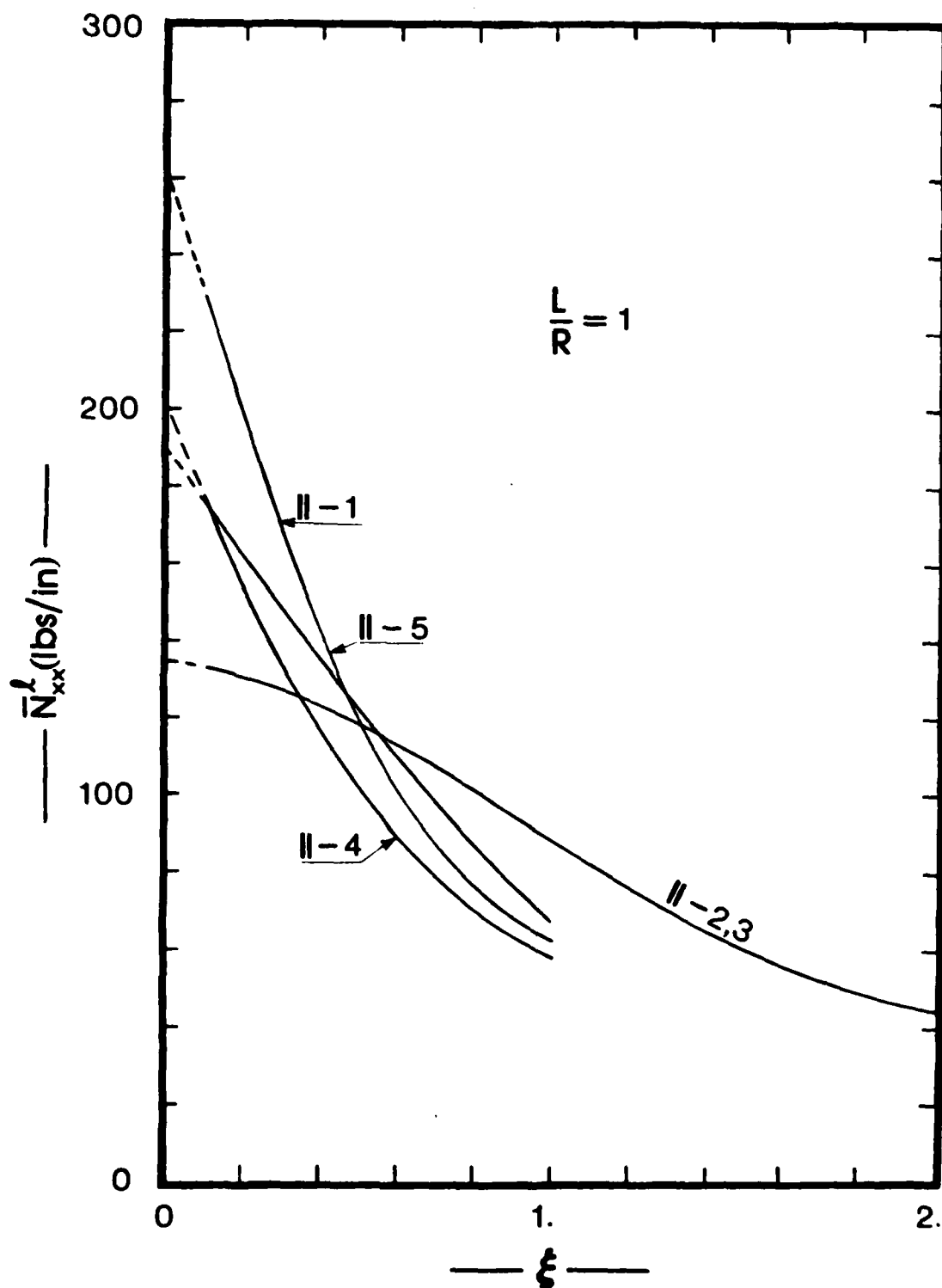


Fig. 10. Critical Conditions for II-i Geometries;
Uniform Axial Compression; $L/R = 1$
(SS-3; Axisymmetric Imp.)

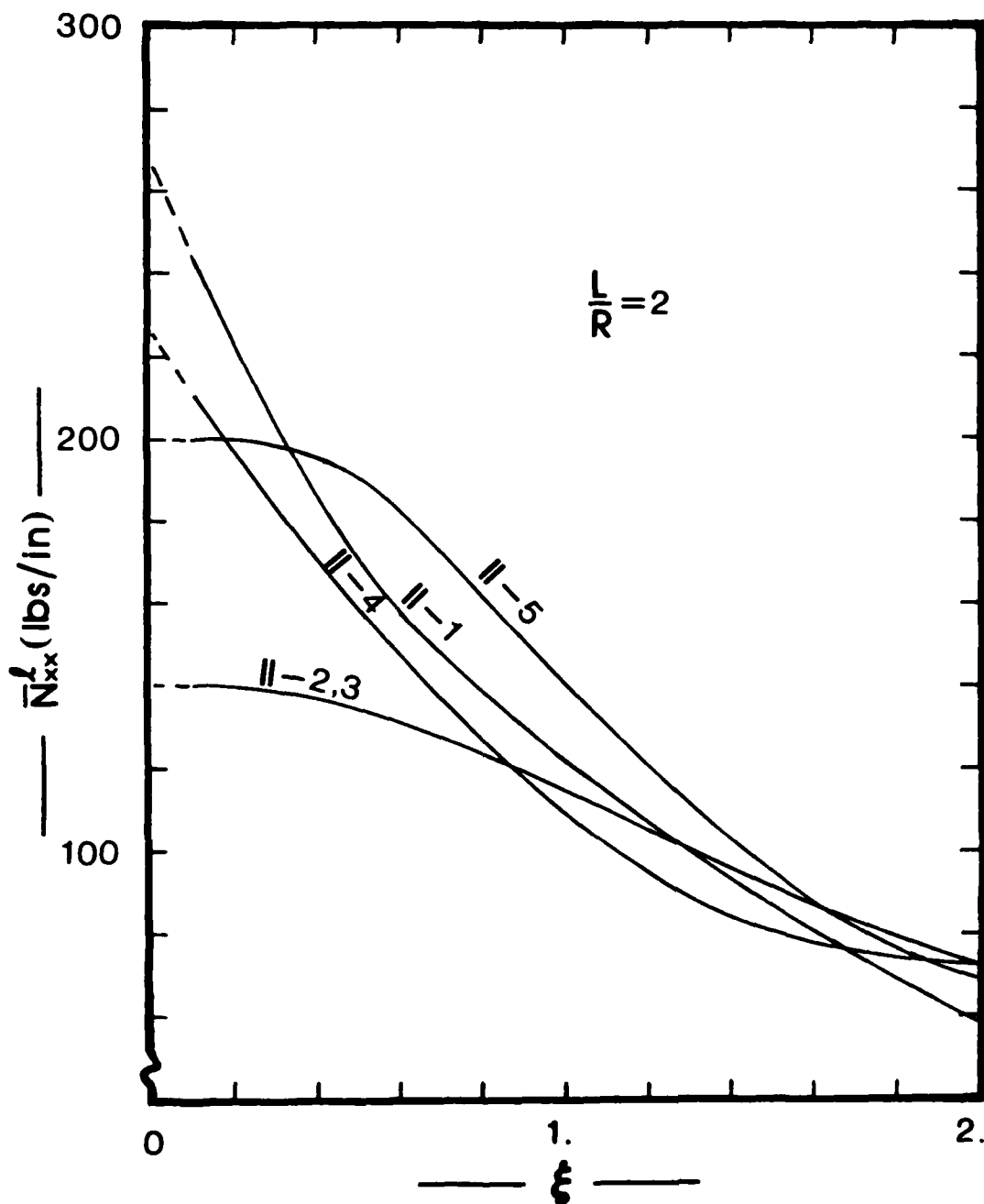


Fig. 11. Critical Conditions for II-i Geometries;
Uniform Axial Compression; $L/R = 2$
(SS-3; Axisymmetric Imp.)

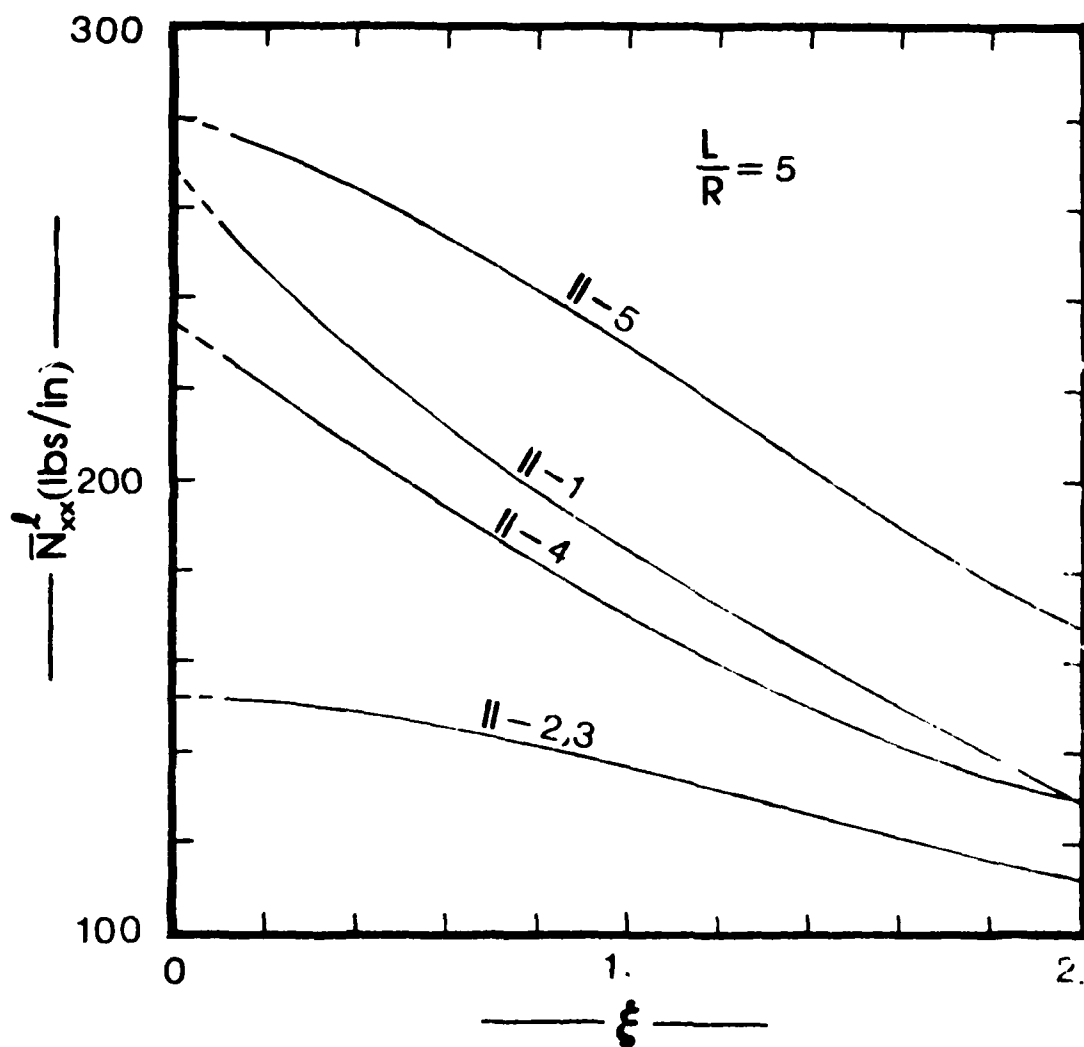


Fig. 12. Critical Conditions for II-i Geometries
Uniform Axial Compression; $L/R = 5$
(SS-3; Axisymmetric Imp.)

antisymmetric laminate is not the best layup for resisting axial compression.

Table 7 presents critical loads for geometries I-i subjected to torsion. The results are also presented graphically on Figs. 13-15. The reader is reminded that the imperfection shape for this load case is similar to the linear theory eigenmode (see Ref. 15) and it is L/R -dependent. Regardless of the shape, the imperfection parameter, ξ , is equal to w_{\max}/h . For all L/R values the I-1 geometry seems to be the weakest one. On the other hand, geometry I-5 yields the strongest configuration. For $L/R = 1$ the I-2,3 configurations seem strong, but as L/R increases they become weaker by comparison to the asymmetric configurations. If torsion were to be reversed the strength of the I-2,3 configurations would remain unchanged (the role of I-2 and I-3 would be interchanged), while the asymmetric configurations could change for the worse. The reason for this expectation is that for positive torsion, tension is expected along a direction making a positive angle with the x-axis (for isotropic construction it would have been $\approx 45^\circ$). The fibers are placed from 0° to 90° or from 90° to 0° in the various layers of I-5 and I-4. Thus, the tensile unidirectional strength of the fibers is utilized. If the torsion is reversed, these same fibers would tend to be in compression and this would imply that I-4 and I-5 are weaker for negative torsion than for positive torsion. Of course no mention is made of the effect of the (negative torsion) imperfection shape. This could be a totally separate study. Along these lines, note that the I-1 geometry (see Ref. 15) is stronger when loaded in the negative direction than in the positive direction, provided that the imperfection shape is similar to the positive torsion buckling mode.

TABLE 7. CRITICAL LOADS; TORSION
(I - i GEOMETRIES)

Geometries	ξ	\bar{N}_{xy}^L in lbs/in (wave No. at Limit Pt.)		
		L/R = 1	L/R = 2	L/R = 5
I - 1	0.1	55.34 (15)	35.32 (11)	21.00 (7)
	0.5	45.36 (15)	31.57 (11)	19.43 (7)
	1.0	43.62 (15)	28.32 (11)	18.01 (7)
I - 2	0.1	78.90 (13)	46.4 (9)	24.91 (6)
	0.3	73.16 (13)	-	-
	0.5	66.36 (13)	41.81 (9)	23.15 (6)
	1.0	-	37.89 (9)	21.57 (6)
I - 3	0.1	79.34 (13)	46.36 (9)	24.84 (5)
	0.3	73.41 (13)	-	-
	0.5	66.50 (13)	41.84 (9)	23.08 (6)
	1.0	-	37.96 (9)	21.51 (6)
I-4	0.1	56.69 (16)	44.18 (12)	29.81 (8)
	0.5	45.91 (15)	38.75 (12)	27.16 (8)
	1.0	39.51 (14)	34.22 (12)	24.74 (8)
I-5	0.1	84.83 (16)	66.49 (12)	42.91 (8)
	0.5	64.20 (16)	56.91 (12)	38.50 (8)
	1.0	46.79 (15)	48.72 (12)	34.27 (8)

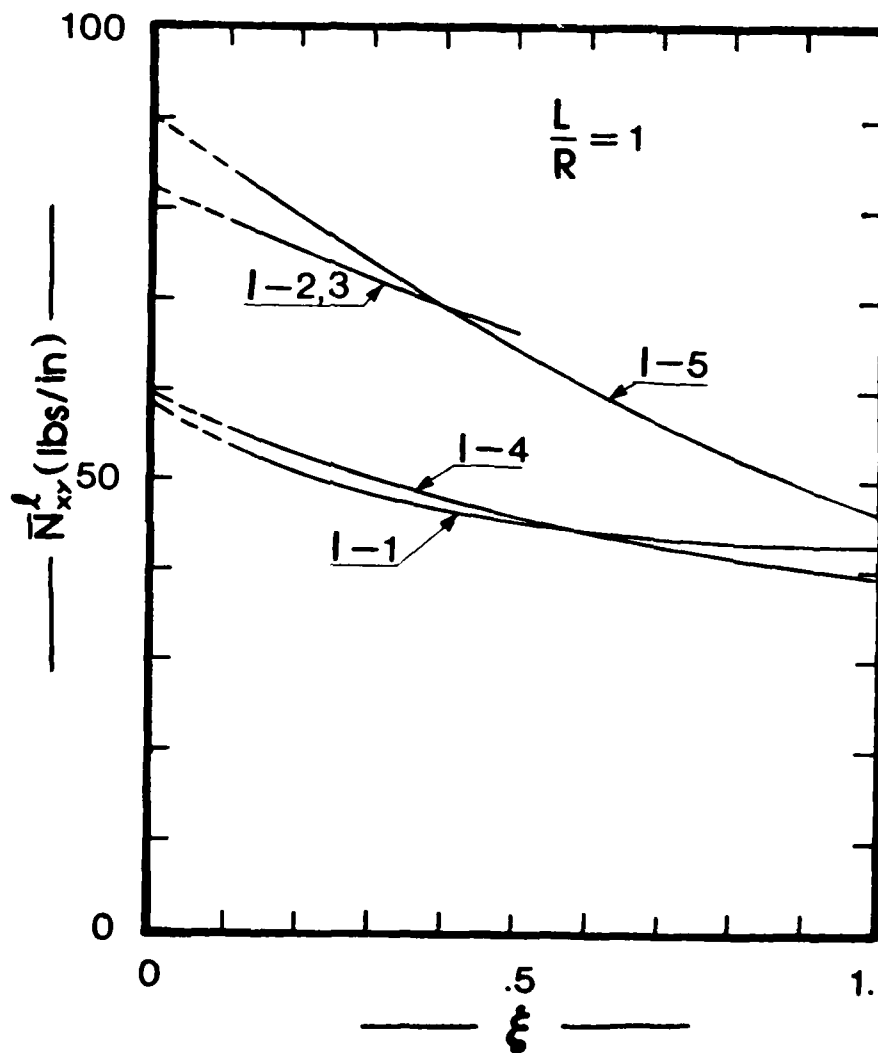


Fig. 13. Critical Conditions for I-1 Geometries; Torsion; $L/R = 1$ [(SS-3; Imp. - Eq. (29a)]

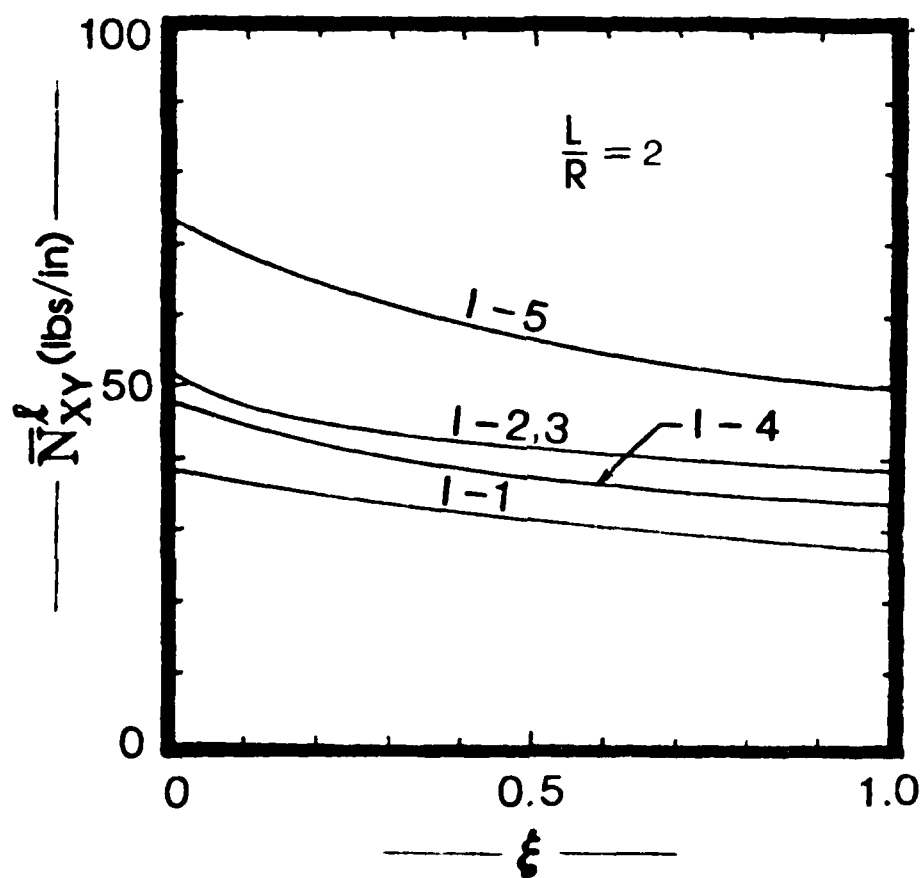


Fig. 14. Critical Conditions for I-i Geometries;
Torsion; $L/R = 2$ [SS-3; Imp. - Eq. (30)].

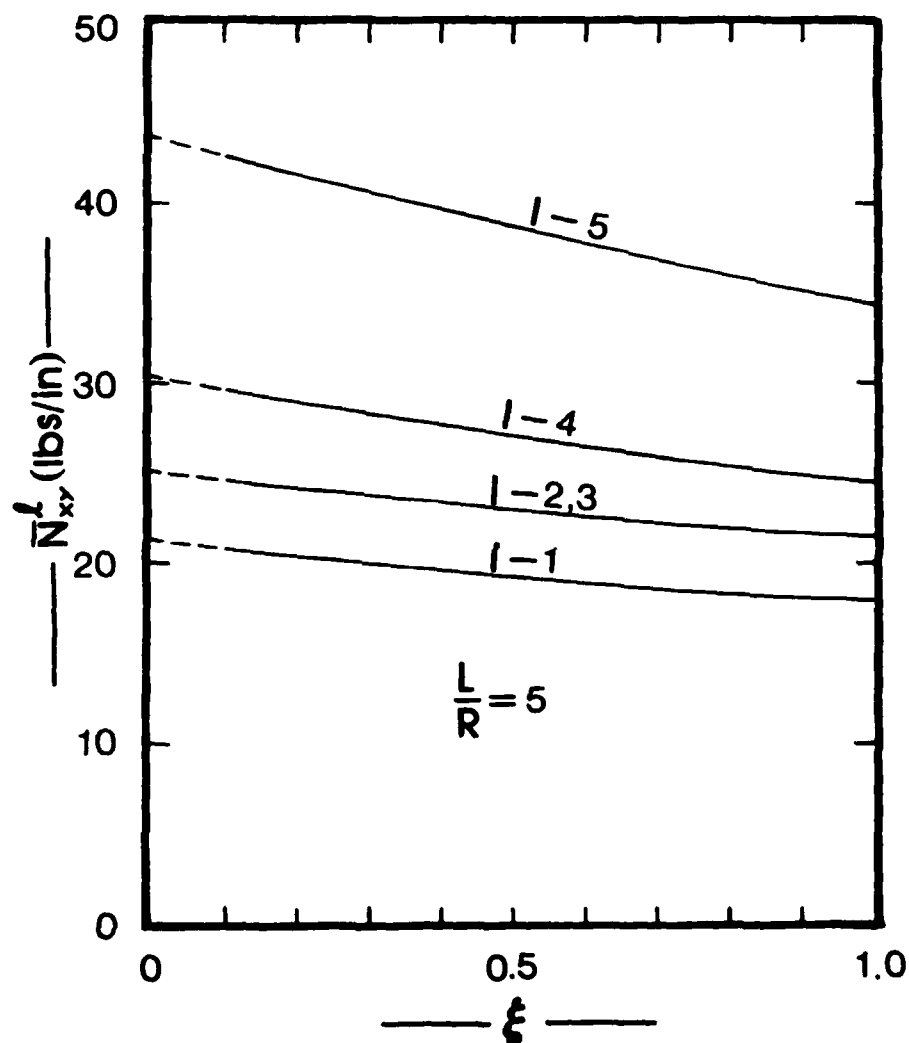


Fig. 15. Critical Conditions for I-1 Geometries;
Torsion; $L/R = 5$ [SS-3; Imp. - Eq. (31)]

TABLE 8. CRITICAL LOADS: TORSION
(II-i GEOMETRIES)

Geometry	ξ	$\frac{-\ell}{N_{xx}}$ in lbs/in (wave No. at Limit Pt)		
		L/R = 1	L/R = 2	L/R = 5
II-1	0.1	53.54 (18)	38.49 (13)	25.50 (9)
	0.5	43.49 (17)	31.74 (13)	23.10 (9)
	1.0	40.15 (17)	27.17 (13)	20.92 (9)
II-2	0.1	82.46 (14)	48.25 (9)	26.17 (6)
	0.3	73.194 (13)	-	-
	0.4	69.76 (12)	-	-
	0.5	-	42.43 (9)	24.50 (6)
	1.0	-	37.31 (9)	23.00 (6)
II-3	0.1	82.12 (13)	48.25 (9)	26.22 (6)
	0.3	73.07 (13)	-	-
	0.4	69.69 (13)	-	-
	0.5	-	42.45 (9)	24.55 (6)
	1.0	-	37.40 (9)	23.06 (6)
II-4	0.1	57.13 (16)	44.11 (12)	29.69 (8)
	0.5	44.23 (15)	37.73 (12)	27.36 (8)
	1.0	37.46 (15)	32.54 (11)	25.29 (8)
II-5	0.1	81.19 (16)	63.61 (13)	41.96 (8)
	0.5	56.42 (16)	52.33 (12)	38.10 (8)
	1.0	42.23 (14)	41.38 (13)	34.51 (8)

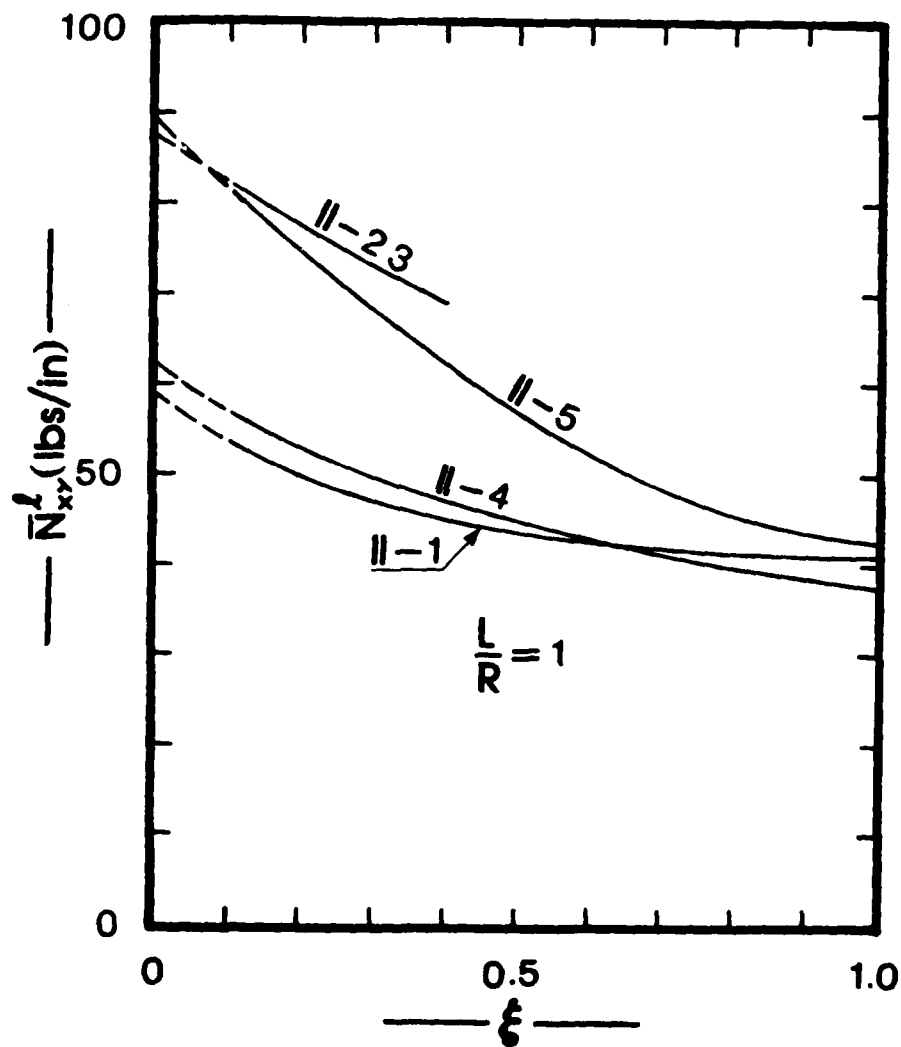


Fig. 16. Critical Conditions for II-1 Geometries; Torsion; $L/R = 1$ [SS-3; Imp. - Eq. (29b)]

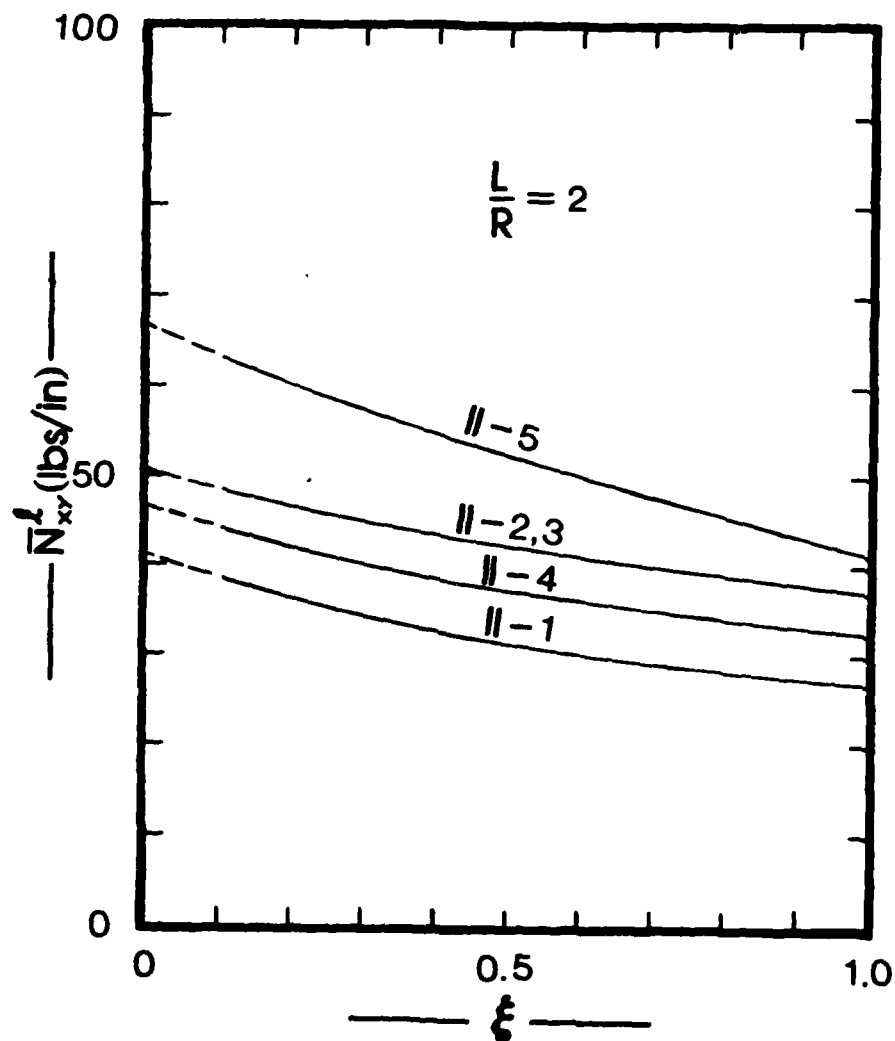


Fig. 17. Critical Conditions for II-i Geometries; Torsion; $L/R = 2$ [SS-3; Imp.- Eq. (30)].

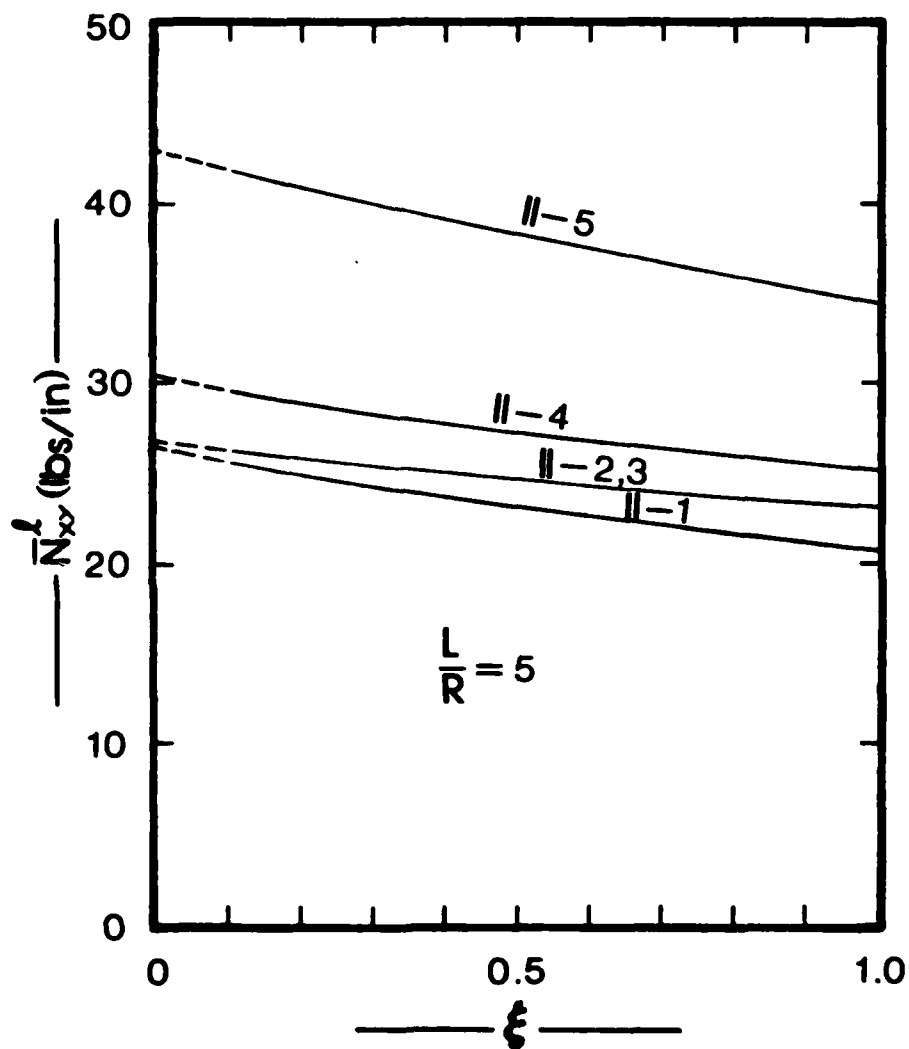


Fig. 18. Critical Conditions for II=1 Geometries;
Torsion; $L/R = 5$ [SS-3; Imp. - Eq. (31)].

Table 8 presents critical torques for geometries II-i. The results are also presented graphically on Figs. 16-18. The conclusions are very similar to those for geometries I-i. There is one important observation though derived from the comparison of the two groups. Since both groups have the same total thickness (0.0212 in.) and radius (7.5 in.) use of more layers (from four to six) increases the load carrying capacity for the antisymmetric configurations (II-2,3 versus I-2,3), but it decreases it for the asymmetric configuration II-5 (it can even be said for II-4). The comparison between II-1 and I-1 is not valid, since II-1 contains two 0°-plies (outer and inner), while I-1 has no such plies.

Finally, when the curves (see Figs. 13 and 16) terminate at $\xi = 0.5$, it means that no limit point could be found for higher ξ -values.

Experimental results do exist for some of the configurations discussed in this section (see Ref. 21). These along with other experimental findings are discussed in the next section.

IV.3 Comparison with Experimental Data

The best means for establishing confidence in an analytical method is to compare it with experimental results, obtained by researchers not connected in any manner with those who developed the analytical procedure.

The purpose of the present section is to present such a comparison. The literature was searched and two sets of experimental results are found; (a) those for which the imperfect geometry is described in terms of imperfection shape and amplitude and (b) those for which there is no data describing the initial geometric imperfection. Moreover, the load cases considered are uniform axial compression and torsion, applied either individually or in combination.

The comparison for class (a) (above) is direct, because both the shape and the amplitude of the initial geometric imperfection are known. On the other hand for class (b) geometries, the comparison is made by assuming a shape for the initial geometric imperfection and by varying the amplitude from some small fraction of the total thickness (five or ten percent to approximately 50% of the total thickness). Clearly, for this latter class of imperfect geometries, the comparison is more qualitative.

IV.3.1 Description of Geometry

Experimental results, used herein for comparison with theoretical predictions, are obtained from four sources. The first source is an unpublished paper presented by Professor Shigeo Kobayashi at the AIAA/ASME/ASCE/AHS 23rd SDM Conference in New Orleans in 1982 (Ref. 24). The presentation took place in a "Work in Progress" session (structures). At this presentation the author supplied the audience with an addendum to his abstract which described the experimental results on Graphite-Epoxy Composite cylinders in axial compression. Through this information and private communication that followed, the complete description was secured and is listed herein as Group A. The imperfection amplitude and shape are not known for this group.

The second source (Ref. 25) is a 1976 University of Toronto report in which analytical and experimental results are given for imperfect Glass/Epoxy cylinders subjected to combined loading. Only one set of results is employed herein and it is listed as Group B. Information concerning the imperfection shape and amplitude is provided by the author and listed below. The load case for this group is a combined application of axial compression and torsion.

The third source is a 1974 AIAA Paper (Ref. 21) which presents experimental results for Boron/Epoxy and Graphite/Epoxy imperfect cylinders subjected to axial compression and torsion, applied either individually or in combination. Certain geometries, from this reference are employed herein. These configurations are listed below as Group C. Information is not provided for the imperfection shapes and amplitudes.

Finally, the last source is a 1973 Journal of Spacecraft paper (Ref. 26), which describes experimental and theoretical results on axially-loaded Glass/Epoxy imperfect cylinders. This work was also performed at the University of Toronto under the direction of Professor Tennyson. Three geometries from this source are employed herein and they constitute Group D. The imperfection shape and amplitude are supplied by Ref. 26.

In describing each group, information concerning the following is provided: Load case, number of plies, stacking description and order, material and material properties, ply and laminate thickness, length and radius of the laminate, boundary conditions, and information on the geometric imperfection. Each configuration in a group (if more than one) is listed as case-Li, where i is an integer, and L assumes the letters A, B, C and D (group).

Group A (Kobayashi et al - Ref. 24)

1) Load: Uniform Axial Compression

2) Material: Graphite/Epoxy

3) Material Properties: $E_{11} = 17.40 \times 10^6$ psi;

$$E_{22} = 1.115 \times 10^6 \text{ psi}$$

$$G_{12} = 0.707 \times 10^6 \text{ psi}$$

$$\nu_{12} = 0.32$$

- 4) Diameter and Length: $2R = 7.874$ in.; $L = 7.874$ in.
- 5) Boundary Conditions: CC-4 ($u = \bar{u}$, $v = w = w_{,x} = 0$)
- 6) Imperfection: No information. So far, the data are common for all cases.

Case-A1: A three-ply laminate ($90^\circ/-20^\circ/20^\circ$)

$$h_{\text{ply}} = 0.0055 \text{ in.}, h = 0.0165 \text{ in.}$$

Case-A2: A four-ply laminate ($90^\circ/-45^\circ/-45^\circ/0^\circ$)

$$h_{\text{ply}} = 0.0057 \text{ in.}, h = 0.0228 \text{ in.}$$

Case-A3: A six-ply laminate ($90^\circ/90^\circ/30^\circ/-30^\circ/-30^\circ/30^\circ$)

$$h_{\text{ply}} = 0.0059 \text{ in.},$$

$$h = 0.0354 \text{ in.}$$

Note that all three configurations are asymmetric with respect to the midsurface.

The stacking order starts from the outside of the cylinder and moves inward. Thus, in case-A1 the outer ply strong axis (of orthotropy) makes a 90° angle with longitudinal axis of the cylinder; the next ply makes a -20° and the inner one a 20° angle with the longitudinal axis.

Case-A4: There is a fourth configuration in this group, for which all data are the same as A1, A2, and A3 except for the material properties, thickness and the sequence of stacking. For this case,

$$E_{11} = 16.78 \times 10^6 \text{ psi}; E_{22} = 0.922 \times 10^6 \text{ psi};$$

$$G_{12} = .707 \times 10^6 \text{ psi}; \nu_{12} = 0.32$$

$h_{\text{ply}} = 0.00667$ in; $h = 0.04$ in. and the stacking sequence for this six-ply laminate is: ($0^\circ/60^\circ/-60^\circ/-60^\circ/60^\circ/0^\circ$)

Note that, unlike the other three configurations in this group, this laminate is symmetric with respect to the midsurface.

Group B (Booton, Ref. 25)

- 1) Load: Combined Axial Compression and Torsion.
- 2) Material: Glass/Epoxy
- 3) Material Properties: $E_{11} = 6.32 \times 10^6$ psi;
 $E_{22} = 1.74 \times 10^6$ psi;
 $G_{12} = 0.78 \times 10^6$ psi;
 $\nu_{12} = 0.435$.
- 4) Diameter and Length; $2R = 13.2$ in.; $L = 12.4$ in.
- 5) Boundary Conditions: CC-4 ($u = \bar{u}$; $v = w = \bar{w} = 0$).
- 6) Imperfection: $w^0(x,y) = (0.28)(0.27) \cos \frac{17\pi x}{L}$
(w^0 is positive inward; axisymmetric imperfection).

Only one configuration is used for this group.

Thus, case-B1: A three-ply laminate ($45^\circ/0^\circ/-45^\circ$)

$h_{\text{ply}} = 0.009$ in.; $h = 0.027$ in.

Group C (Wilkins et al. - Ref. 21)

- 1) Load: Combined Axial Compression and Torsion
- 2) Material: Boron/Epoxy and Graphite/Epoxy
- 3) Material Properties:

(i) Boron/Epoxy	(ii) Graphite/Epoxy
$E_{11} = 30.0 \times 10^6$ psi	$E_{11} = 2.17 \times 10^6$ psi
$E_{22} = 2.7 \times 10^6$ psi	$E_{22} = 1.44 \times 10^6$ psi

$$G_{12} = 0.65 \times 10^6 \text{ psi} \quad G_{12} = 0.65 \times 10^6 \text{ psi}$$

$$\nu_{12} = 0.21 \quad \nu_{12} = 0.28$$

- 4) Diameter and Length: $2R = 15 \text{ in.}; L = 15 \text{ in.}$
- 5) Boundary Conditions: SS-3 ($N_{xx} = \bar{N}_{xx}; v = w = M_{xx} = 0$)
- 6) Imperfection: No information

So far, the data are common for all cases.

Case-C1: A four-ply Boron/Epoxy laminate

$$(45^\circ/-45^\circ/-45^\circ/45^\circ) \quad h_{\text{ply}} = 0.0053 \text{ in.}$$

$$h = 0.212 \text{ in.}$$

Case-C2: A six-ply Graphite/Epoxy laminate

$$(0^\circ/45^\circ/-45^\circ/-45^\circ/0^\circ)$$

$$h_{\text{ply}} = 0.0056 \text{ in.}, h = 0.336 \text{ in.}$$

Note that both configurations are symmetric about the laminate midsurface.

As in Group A, the stacking sequence starts from the outside and moves inward.

Group D (Tennyson and Muggeridge, Ref. 26)

- 1) Load: Uniform Axial Compression
- 2) Material: Glass/Epoxy "Skotchply" (XP250)
- 3) Material Properties: The properties are given separately for each configuration.
- 4) Diameter and Length: $2R = 12.5 \text{ in.}, L = 12.45 \text{ in.}$
- 5) Boundary Conditions: CC-4 ($u = \bar{u}; v = w = w_{,x} = 0$).
- 6) Imperfection: $w^0(x,y) = \frac{1}{2} h \cos \frac{\pi x}{L}$

Note that the laminate thickness (h) wave number (m) and imperfection amplitude (ξ) depend on the configurations (case). Furthermore, the imperfection shape for all configurations, is axisymmetric.

The above data are common to all cases

Case-D1: A three-ply Glass/Epoxy laminate ($0^\circ/70^\circ/-70^\circ$)

$$E_{11} = 5.03 \times 10^6 \text{ psi}; E_{22} = 2.58 \times 10^6 \text{ psi};$$

$$G_{12} = 0.837 \times 10^6 \text{ psi}; \nu_{12} = 0.345$$

$$h_1 = h_2 = h_3 = 0.009 \text{ in (} h_i \text{ thickness of each ply;}$$

from outer to inner: 1, 2, 3).

$$h = 0.027 \text{ in.} \quad = 0.0468$$

$$(\xi = w_{\max}^0/h); m = 18 \text{ (see the imperfection expression);}$$

Case 1a of Ref. 26.

Case-D2: A three-ply Glass/Epoxy laminate ($45^\circ/-45^\circ/90^\circ$)

$$E_{11} = 6.109 \times 10^6 \text{ psi};$$

$$E_{22} = 2.69 \times 10^6 \text{ psi}; G_{12} = 0.517 \times 10^6 \text{ psi};$$

$$\nu_{12} = 0.317$$

$$h_1 = 0.009 \text{ in}; h_2 = h_3 = 0.0092 \text{ in}; h = 0.274 \text{ in.}$$

$$\xi = 0.034; m = 18; \text{ case 4a of Ref. 26}$$

Case-D3: A three-ply Glass/Epoxy laminate ($30^\circ/90^\circ/30^\circ$)

$$E_{11} = 5.42 \times 10^6 \text{ psi}; E_{22} = 2.6 \times 10^6 \text{ psi};$$

$$G_{12} = 0.687 \times 10^6 \text{ psi}; \nu_{12} = 0.365$$

$$h_1 = h_3 = 0.009 \text{ in.}, h_2 = 0.0093 \text{ in.}; h = 0.0273 \text{ in.}$$

$$\xi = 0.0304; m = 17; \text{ case 11a of Ref. 26.}$$

Note that all three configurations are asymmetric. Moreover, all data are taken from Ref. 26. In Ref. 26, the imperfection (axisymmetric) is given in the form of

$$w^0(x) = \xi h \cos \frac{qx}{R} \quad (32)$$

where the number q is given (Ref. 26). The imperfection expression is changed, herein, to be compatible with Eqs. (12).

The solution methodology described in Ref. 15 is employed to compute critical (limit point) loads which are then compared to the experimental results. This is easily done for the configurations for which the imperfection shape and amplitude are fully described.

For the geometries, for which no information concerning the imperfection is given, the comparison is more qualitative.

IV.3.2. Theoretical Results and Discussion

The theoretical predictions, based on the solution scheme of Ref. 15, and the comparison with the experimental results is discussed separately for each group of configurations.

Group A

Since no information is provided (for this group), concerning the amplitude and shape of imperfection, the comparison is expected to be more qualitative than quantitative. It is assumed that the shape of imperfection is almost axisymmetric and the amplitude of imperfection is varied

from a small fraction of the thickness to almost one thickness of the laminate.

$$w^0(x,y) = -\frac{1}{3}h \left(\cos \frac{2\pi x}{L} + 0.1 \sin \frac{\pi x}{L} \cos \frac{\pi y}{R} \right) \quad (28)$$

Note that $|w_{\max}| = 1.1 \frac{1}{3} h$, where h is the laminate thickness.

Both the theoretical and the experimental results are presented in tabular form (see Table 9).

On Table 9, the buckling load and the observed circumferential wave number are listed on columns two and three (data from Ref. 24). The next three columns contain theoretical results for three values of the imperfection amplitude parameter ξ . For case-A1, the comparison suggests that the maximum imperfection amplitude for the tested geometry might be larger than one laminate thickness. Note that when $\xi = 1$ ($w^0_{\max}/h = 1.1$) the theoretical load is 133.83 lbs/in.

For case A2, the comparison suggests, that the "tested geometry" maximum imperfection amplitude is (approximately) 0.9 h .

Finally, the comparison for the other two cases (A2 and A4) is much better, since it suggests that the maximum imperfection amplitude is 0.4 h . Again, it is stressed, that for this group the comparison is rather qualitative.

Group B

Only one geometry is taken from Ref. 25. According to this reference, the imperfection is axisymmetric and experimental results are reported for a combined application of uniform axial compression and torsion. Moreover, theoretical predictions are reported in Ref. 25, which are obtained by employing a solution scheme that assumes axisymmetric prebuckling behavior and finding bifurcation loads corresponding to asymmetric behavior.

TABLE 9. THEORETICAL AND EXPERIMENTAL RESULTS FOR GROUP A

Geometry	Experimental			Theoretical			
Case-	$\frac{-l}{N_{xx}}$	$\frac{\text{lbs.}}{\text{in.}}$	n wave No.	$\frac{-l}{N_{xx}}$	$\frac{\text{lbs.}}{\text{in.}}$	n wave No.	ξ : Imp. Amplitude
A1	120.56	10		151.19		12	0.3
				140.55		12	0.5
				133.83		12	1.0
A2	248.46	8		362.30		9	0.1
				294.54		9	0.5
				231.83		9	1.0
A3	802.99	-		945.78		9	0.1
				872.99		9	0.3
				792.91		9	0.5
A4	892.02	-		944.66		10	0.2
				895.38		10	0.3

The present results, along with the theoretical predictions of Ref. 25 and the experimental findings are presented graphically on Fig. 19. It is clearly seen from this figure that the agreement is very good.

Group C

For this particular group there is no information concerning the amplitude and shape of imperfection. It is important then, to employ some shape for the imperfection and vary the imperfection amplitude in order to accomplish some comparison (qualitative) with the experimental results (Ref. 21).

Because the loading consists of both axial compression and torsion, three imperfection shapes are initially employed. First, a virtually axisymmetric imperfection is used, which is characterized by Eq. (28).

The other two shapes, used for the imperfection, correspond to approximations of the linear theory (Ref. 15) buckling modes for positive and negative torsion.

In particular, one of the Appendices of Ref. 15 deals with solutions to the linearized buckling equations for the case of pure torsion. The Galerkin procedure is employed and the following approximate form, for the buckling mode, w^1 , is employed:

$$w^1(x, y) = \sum_{n=0}^N \sum_{m=1}^M \left(A_{mn} \cos \frac{ny}{R} + B_{mn} \sin \frac{ny}{R} \right) X \quad (33)$$

$$\left[\frac{L}{m\pi} \sin \frac{m\pi x}{L} - \frac{L}{(m+2)\pi} \sin \frac{(m+2)\pi x}{L} \right]$$

Because of orthogonality only one n -value is needed. A ten-term approximation ($m = 5$) is obtained in Ref. 15. By studying the results it

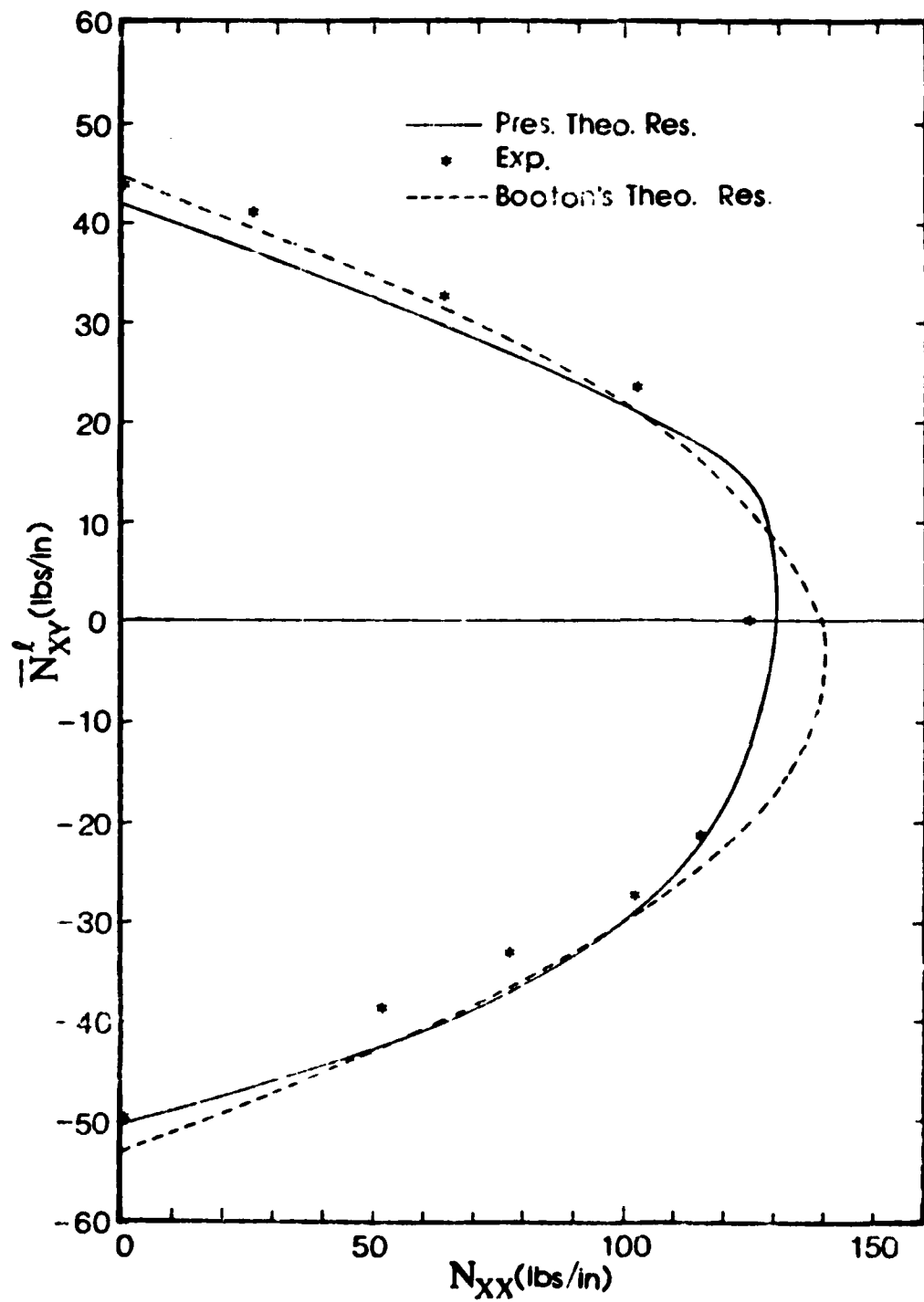


Fig. 19. Critical (Theoretical) and Buckling (Experimental) Loads for Group B

is observed that the linear theory buckling mode is well approximated by two terms. This is accomplished by normalizing all coefficients, in the ten-term approximation, with respect to B_{2n} . A comparison of the order of magnitude of these coefficients yields that all are negligibly small except two. Finally, these two remaining coefficients are adjusted such that the maximum amplitude is $\frac{1}{3}h$. Thus, one two-term approximation is used for positive torsion, $w^o(+)$, and one two-term approximation for negative torsion, $w^o(-)$. These expressions are (applicable to both configurations; cases C1 and C2).

$$w^o(+) = \frac{1}{3}h \left[0.537 \cos \frac{\pi y}{R} \left(\sin \frac{\pi x}{L} - \frac{1}{3} \sin \frac{3\pi x}{L} \right) - 0.671 \sin \frac{\pi y}{R} \left(\sin \frac{2\pi x}{L} - \frac{1}{2} \sin \frac{4\pi x}{L} \right) \right] \quad (34)$$

$$w^o(-) = \frac{1}{3}h \left[0.583 \cos \frac{\pi y}{R} \left(\sin \frac{\pi x}{L} - \frac{1}{3} \sin \frac{3\pi x}{L} \right) + 0.648 \sin \frac{\pi y}{R} \left(\sin \frac{2\pi x}{L} - \frac{1}{2} \sin \frac{4\pi x}{L} \right) \right] \quad (35)$$

Note that, for both expressions (by design)

$$w_{\max}^o / h = \frac{1}{3} \quad (36)$$

The generated results for each configuration are presented (in part) both in graphical and tabular form. Each configuration is treated separately.

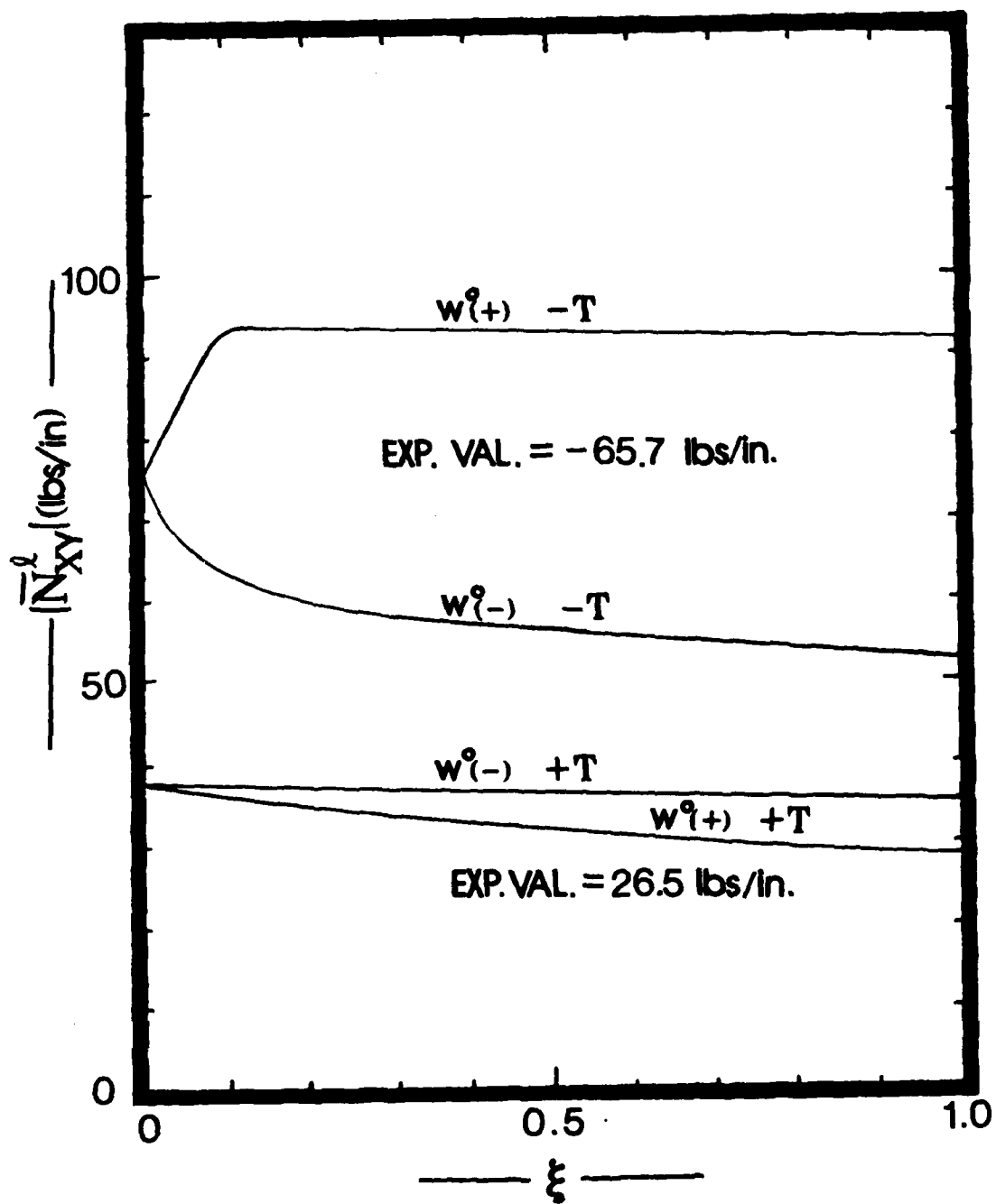


Fig. 20. $-l N_{xy}$ vs. ξ (Imp. Ampl. Parameter)

For Two Imp. Shapes [Eqs. (34) and (35)]

Case C-1: For the case of pure torsion, theoretical predictions are generated for the two imperfection shapes, Eqs. (34) and (35), and for positive and negative torsion for each shape. These theoretical predictions are shown as plots of the value of the critical (limit point) torsion $|\bar{N}_{xy}|$, versus the imperfection amplitude parameter, ξ , on Fig. 20. Note that as the imperfection amplitude approaches zero the results corresponding to the two shapes $w^0(+)$ and $w^0(-)$, approach the same value (as they should). Moreover, it is seen that the shape corresponding to Eq. (34) has a stabilizing effect for small values of ξ and for negative torsion.

The experimental values for positive and negative torsion are also listed on Fig. 20. Note that, for positive torsion the experimental value is 26.5 lbs/in, and the comparison with the theoretical result suggests that the imperfection amplitude is a little larger than one laminate thickness. On the other hand, for negative torsion, the experimental value is 65.7 lbs/in. and the comparison suggests that the imperfection amplitude is less than two tenths of the laminate thickness.

In addition, Ref. 21 provides experimentally obtained, buckling interaction curves (\bar{N}_{xx} vs \bar{N}_{xy}) for this geometry. Again since the imperfection is not known, theoretical interaction curves are obtained analytically for two shapes of imperfection. Eqs. (28) and (34) and various values for the imperfections amplitude parameter, ξ . This comparison is for positive torsion and the results are shown graphically on Figs. 21 and 22. The experimental data are shown by the dashed line.

For this case the comparison must be viewed as qualitative rather than quantitative.

Case - C2: For this six-ply symmetric laminate, a qualitative type of comparison is presented only for positive torsion. The results are, in part, presented graphically on Fig. 23 and in tabular form on Table 10.

Table 10 shows theoretical results obtained by the present analysis, for two imperfection amplitude parameter values ($\xi = 0.05$ and $\xi = 0.50$) and the shape characterized by Eq. (34). First, the critical values corresponding to individual application of the loads are obtained and then the interaction curve is completed by assigning values for the applied torsion and finding the corresponding critical (limit point) axial compression. Note that the assigned values for the torsion are smaller than the individually applied critical torsion.

TABLE 10. CRITICAL CONDITIONS FOR CASE - C2

$\xi = 0.05$	$\bar{N}_{xx} \ell$ lbs/in.	442.6	348.1	232.3	70.32	0
	$\bar{N}_{xy} \ell$ lbs/in.	0	20	40	60	76.4
	n	13	13	12	13	12
$\xi = 0.50$	$\bar{N}_{xx} \ell$ lbs/in.	328.3	262.5	70.5	0	-
	$\bar{N}_{xy} \ell$ lbs/in.	0	15	14	61.4	-
	n	12	14	12	12	

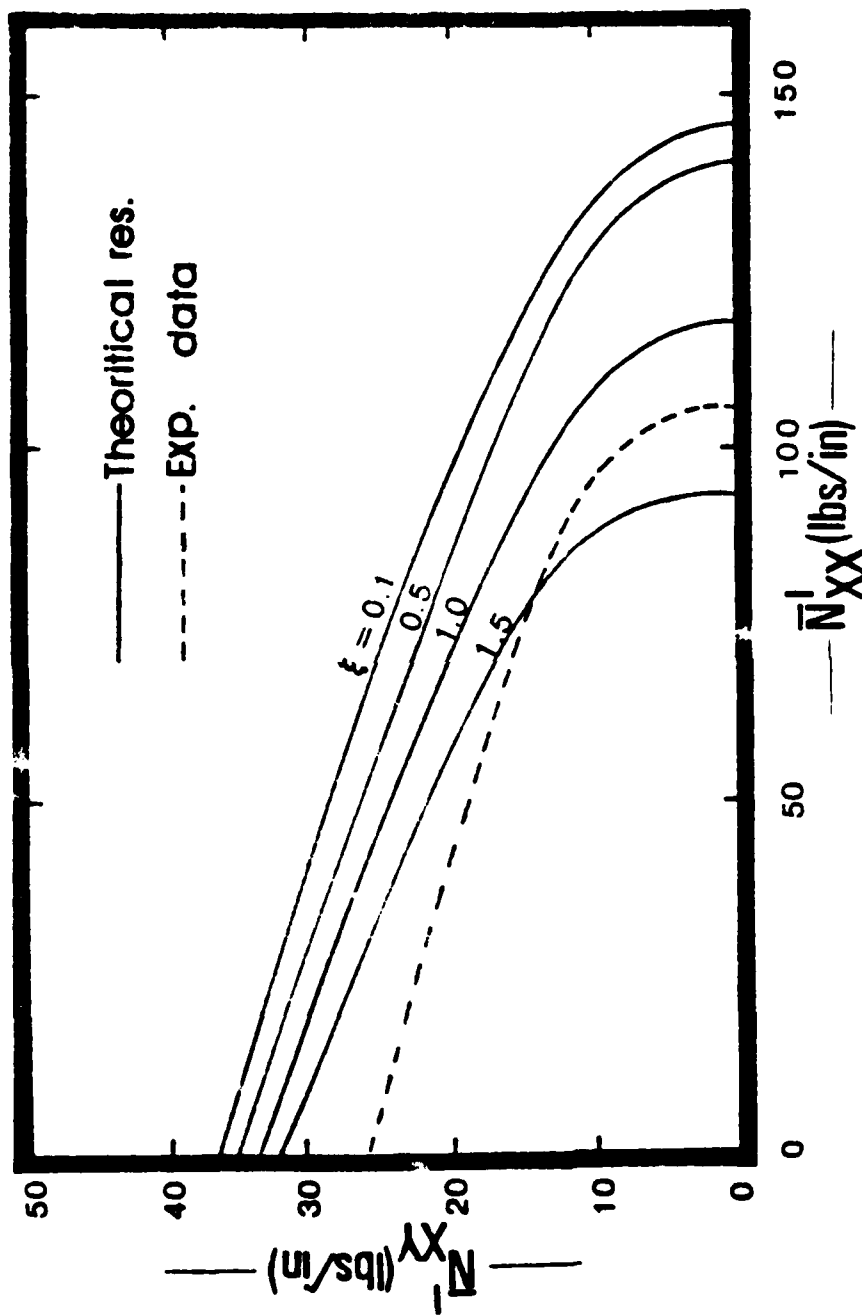


Fig. 21. Critical Interaction Curves
 [Geometry C1(I-1); Axisym. Imp. - Eq. (28)]

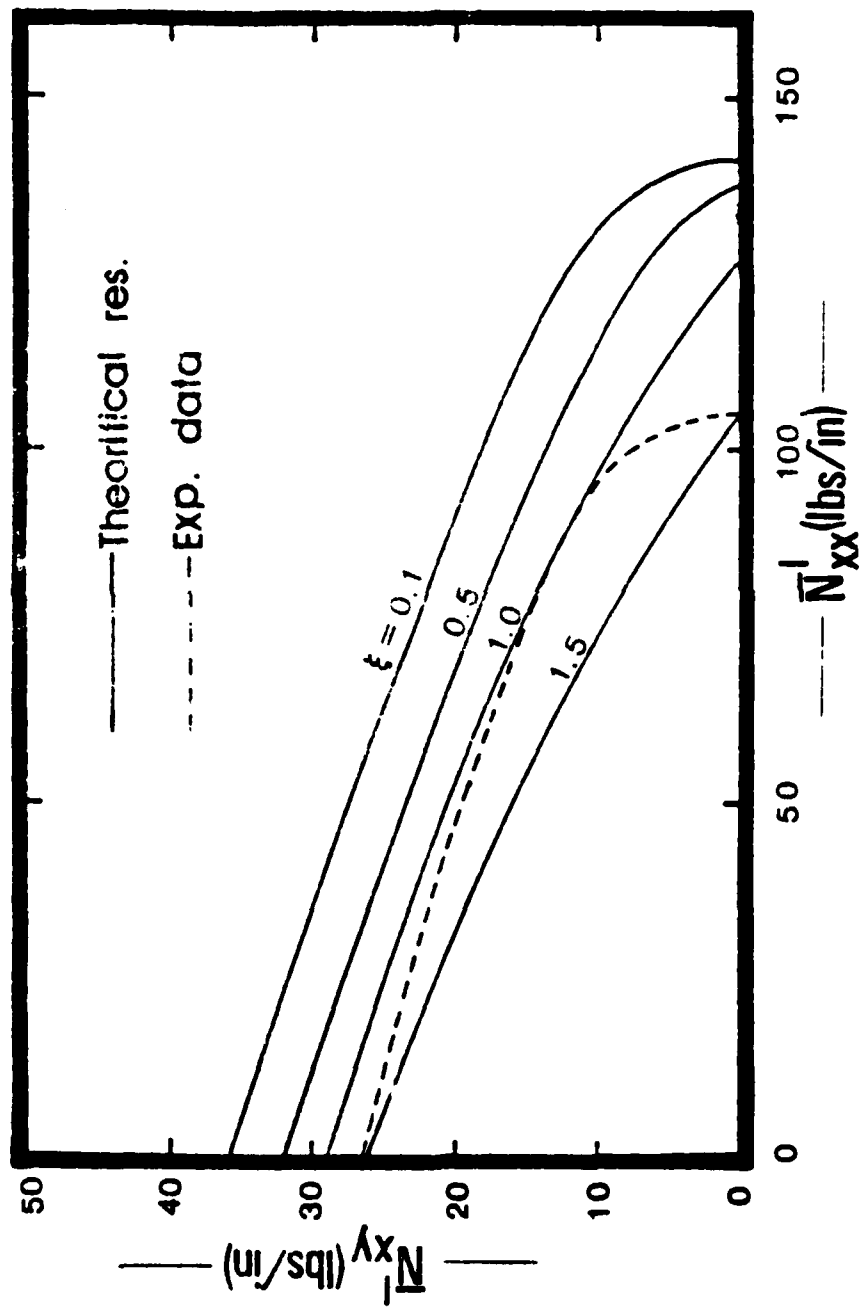


Fig. 22. Critical Interaction Curves
 [Geometry C1 (I-1); Imp. $w^0(+)$ - Eq. (34)]

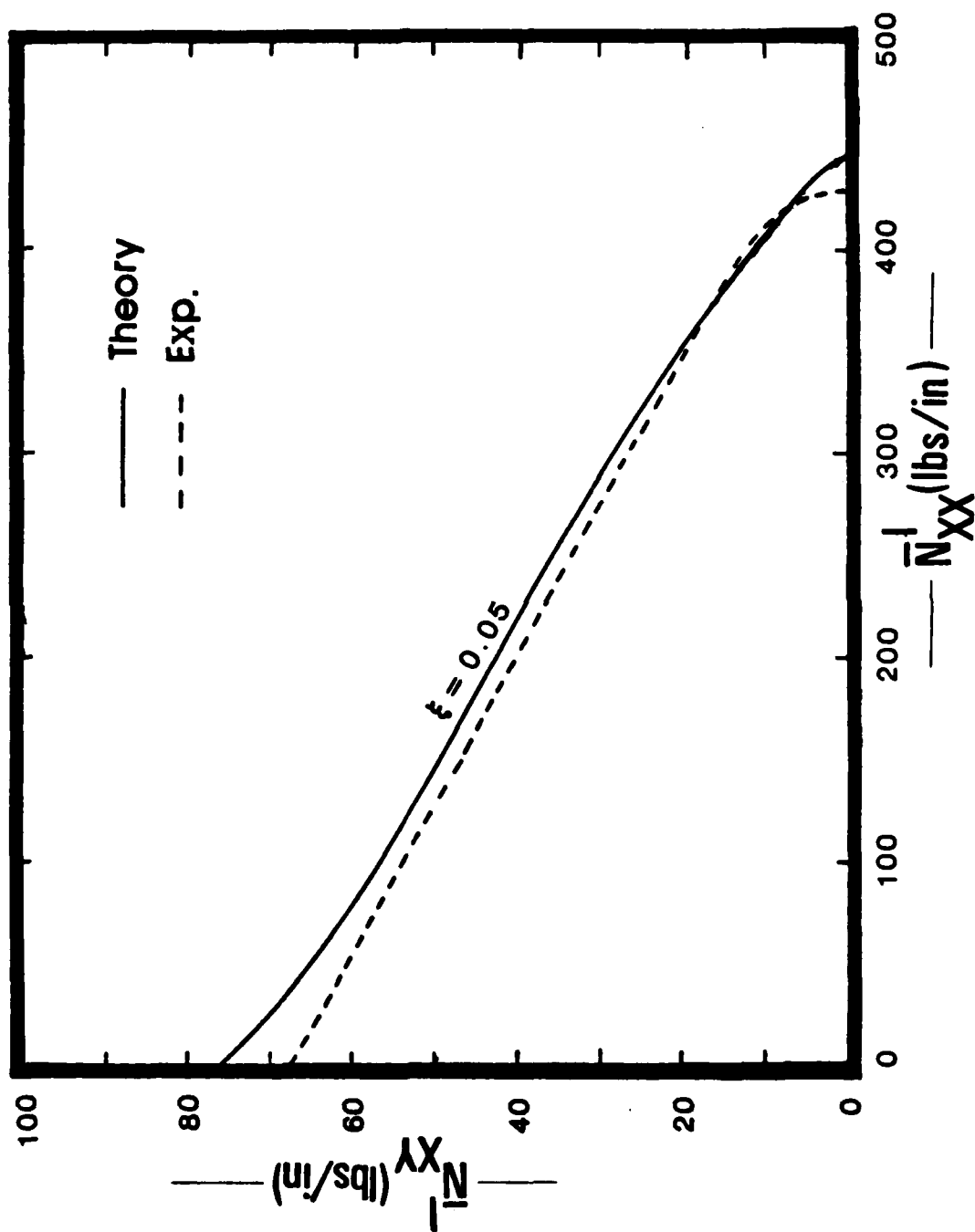


Fig. 23. Critical Interaction Curves

[Geometry C2 (II-1); Imp. $w^0(+)$ - Eq. (34)]

On Fig. 23 the experimental results of Ref. 21, and only the theoretical prediction corresponding to $\xi = 0.05$ are shown. The two curves seem to be very close for the entire range of interest. Thus, the comparison between experimental and theoretical interaction curves seems to be reasonable for this geometry.

Group D

There are several tests reported in Ref. 26. In all of these tests, the imperfection is axisymmetric and theoretical critical loads are reported in Ref. 26, which are obtained by employing a linearized bifurcation analysis. The present methodology is employed and a comparison is made through Table 11. In this table, the geometry, Ref. 26 results, and the present critical loads are listed.

For the first geometry (case-D1), the agreement between experiment (buckling load) and present theory (critical load) is excellent. The theoretical prediction of Ref. 26 is also very good. For the other two geometries (cases - D2 and D3) the agreement seems to be reasonably good (acceptable). For the same reason, the theoretical prediction of Ref. 26 may also be called reasonably good.

TABLE 11. A COMPARISON BETWEEN THEORY AND EXPERIMENT FOR GROUP D

Geometry Case-	Description of Geometry					Ref. 10 Results			Present Results	
	L in.	h in.	R/h	m	δ	Test No.	\bar{N}_{xx} (lbs/in)		$- \ell$ N_{xx}	$\frac{lbs}{in.}$ n
D1	12.42	0.0270	232	18	0.0468	1a	148.9	153.2	151.2	11
D2	12.45	0.276	267	18	0.0340	4a	142.0	165.1	174.5	11
D3	12.43	0.0273	229	17	0.0304	11a	149.1	185.2	174.3	11

IV.4 Concluding Remarks

The comments of this section are only related to the work reported in Chapter IV.

The limited parametric studies, reported herein, suggest that, in order to resist uniform axial compression effectively, 0° -plies should be placed at the extreme plies of the laminate (I-4,5, II-1,4,5). Clearly the anti-symmetric $\pm 45^\circ$ layup yields a weak configuration for this load case. On the other hand for torsion, an asymmetric layup (of the type considered here, I-4,5 and II-4, 5) can be very efficient for torsion of a specified direction (say positive), but if the torsion is reversed, its efficiency is in doubt. The antisymmetric $\pm 45^\circ$ layup, though, seems to be efficient for torsion, which is expected to be acting in both directions (for different load conditions, of course). The symmetric layup (I-1 and II-1) seems to be the weaker configuration, for torsion (by comparison to all used herein.)

The comparison with experimental results seems to be rather good. When direct comparisons (quantitative) were possible (groups B and D) the agreement was good. The qualitative comparison can also be considered a success. These comparisons definitely increase one's confidence in the theoretical solution scheme.

CHAPTER V

CONCLUSIONS AND RECOMMENDATIONS

On the basis of the generated results and their assessment certain findings can be reported.

First, theoretical solutions schemes have been developed for analyzing the behavior of stiffened, laminated, thin cylindrical shells with initial geometric imperfections, various boundary conditions and subjected to static or suddenly applied destabilizing loads (eccentric and applied individually or in combination). Behavior includes the establishment of critical conditions and post-limit point response. This is true for the w, F -formulation which is based on Donnell-type of kinematic relations. With the u, v, w -formulation (regardless of the character of the kinematic relations) dynamic critical loads cannot be found, since the solution scheme was not carried to the post-limit point response (it was deemed unnecessary to do so, because it is very expensive in time and money and the expected benefits did not justify this extra effort).

Next, by comparing critical static loads obtained from two different sets of nonlinear kinematic relations (Donnell and Sanders) it is seen that for isotropic constructions or laminates with properties and layups that yield properties similar to isotropic construction ($B_{ij} = 0$ $A_{11} = A_{22}$, $D_{11} = D_{22}$, $A_{13} = A_{23} = D_{13} = D_{23} = 0$) the L/R ratio is the only influencing parameter. This means that the two results are virtually the same for small to moderate values of L/R ($L/R \leq 5$), but they differ by as much as 15% at large L/R values ($L/R \geq 10$).

For orthotropic construction the results are similar to the isotropic case, when the strong direction is along the cylinder axis (0° along

x-axis) but they start having significant differences, even for small L/R - values ($L/R \leq 2$), when the strong direction is in the hoop direction (y-axis). This conclusion is based on axial compression. No assessment is made for other load cases and/or other laminate layups ($\pm 45^\circ$ anti-symmetric, asymmetric etc).

It is important (and therefore recommended) to continue this study and (a) establish which design parameters affect the accuracy, when using Donnell-type of kinematic relations, and (b) establish limits or bounds on these parameters inside which the Donnell equations yield accurate results.

Moreover, even through the use of Donnell equations, more parametric studies are needed (of the type, reported in Chapter IV), in order to enhance our understanding of the buckling behavior of laminated shells, and therefore improve our capability of designing efficient laminated shells.

Finally, the comparison between theoretical predictions and experimentally obtained results serves to increase our confidence in the developed solution scheme. Thus, this solution methodology may confidently be used, especially in the preliminary design stage, because it allows a quick and an inexpensively obtained assessment of the effect of various design variables on the load carrying capacity of thin cylindrical shells (when subjected to destabilizing loads).

REFERENCES

1. Donnell, L. H., "Stability of Thin-walled Tubes under Torsion", National Advisory Committee for Aeronautics (NACA), TR-479, Washington, D.C., 1933.
2. Hoff, N. J., "The Accuracy of Donnell's Equations", Journal of Applied Mechanics, Vol. 22, No. 3, 1955, pp. 329-334.
3. Flugge, W., Static und Dynamik der Schalen, Julius Springer, Berlin, p. 118; or see Stresses in Shells, Springer-Verlag, Berlin, 1962.
4. Dym, C. L., "On the Buckling of Cylinders in Axial Compression", Journal of Applied Mechanics, Vol. 40, No. 2, 1973, pp. 565-568.
5. Koiter, W. T., "General Equations of Elastic Stability for Thin Shells", Muster D. ed., Proceedings, Symposium on the Theory of Shells, University of Houston, Houston, Texas, 1967.
6. Budiansky, B. "Notes on Nonlinear Shell Theory", Journal of Applied Mechanics, Vol. 35, No. 2, 1968, pp. 393-401.
7. Simites, G. J. and Aswani, M., "Buckling of Thin Cylinders under Uniform Lateral Loading", Journal of Applied Mechanics, Vol. 41, no. 3, 1974, pp. 827-829.
8. Sanders, J. L., "Nonlinear Theories of Thin Shells", Quarterly of Applied Mathematics, Vol. 21, 1963, pp. 21-36.
9. Toda, S., "A Note on the Characteristic Roots for Donnell's Linear Buckling Equations", Proceedings of the National Congress for Applied Mechanics, Vol. 28, (November 1978), 1980 (published), pp. 21-31.
10. Koga, T., and Endo, S., "Comparison of Accuracies of Solutions of Linear Shell Theories for Closed Circular Cylinders under Edgewise Loading", Technical Report of National Aerospace Laboratory, Tokyo, NAL TR-SS2T, November, 1978.
11. Microys, H. F., and Schwaighofer, J., "Isotropic Cylindrical Shells under Line Load", Journal of the Engineering Mechanics Division, Proceedings of the American Society of Civil Engineers, Vol. 104, EM2, 1978, pp. 301-317.
12. Schaighofer, J., and Microys, H. F., "Orthotropic Cylindrical Shells under Line Load", Journal of Applied Mechanics, Vol. 46, No. 2, 1979, pp. 356-362.
13. Akeju, T. A. I., "Reduced Thin Shell Equations for Circular Cylinders", Journal of the Engineering Mechanics Division, Proceedings of the American Society of Civil Engineers, Vol. 1979, EM1, 1981, pp. 249-255.

14. El Naschie, M. S., and Hosni, A. F., "A Note on the Accuracy of the Nonlinear Shell Equations in the Postbuckling range", Zeitschrift für Angewandte Mathematik und Mechanik, Vol. 57, No. 11, 1977, pp. 673-674.
15. Simites, G. J., Sheinman, I., and Shaw, D. "Stability of Laminated Composite Shells Subjected to Uniform Axial Compression and Torsion" Interim Scientific Report to the Air Force Office of Scientific Research (Grant No. AFOSR 81-0227), AFOSR TR-82-XXXX, Georgia Institute of Technology, Atlanta, 1982.
16. Baruch, M., and Singer, J., "Effect of Eccentricity of Stiffeners on the General Instability of Stiffened Cylindrical Shells under Hydrostatic Pressure", Journal of Mechanical Engineering Science, Vol. 6, No. 1, 1963, pp. 23-27.
17. Sheinman, I., Shaw, D., and Simites, G. J., "Nonlinear Analysis of Axially-Loaded Laminated Cylindrical Shells", International Journal of Computers and Structures, Vol. 16, No. 1, 1983, pp. 131-137.
18. Jones, R. M., Mechanics of Composite Materials, McGraw-Hill Book Co., Inc., New York, 1975, p. 147.
19. Thurston, G. A., "Newton's Method Applied to Problems in Nonlinear Mechanics" Journal of Applied Mechanics, Vol. 32, 1965, pp. 383-388.
20. Sheinman, I., and Simites, G. J., "Buckling Analysis of Geometrically Imperfect, Stiffened Cylinders under Axial Compression", AIAA Journal, Vol. 15, 1977, pp. 374-382.
21. Wilkins, D. J., and Love, T. S., "Combined Compression Torsion Tests of Laminated Composite Cylindrical Shells", Proceedings of the AIAA/ASME/SAE 15th Structures, Structural Dynamics and Materials Conference, Las Vegas, April 1974, AIAA Paper No. 74-379.
22. Hoff, N. J., and Soong, T. C., "Buckling of Circular Cylindrical Shells in Axial Compression", International Journal of Mechanical Sciences, Vol. 7, 1965, pp. 489-496, (also Stanford University Department of Aeronautics and Astronautics, Report SUDAER No. 204, 1964).
23. Hess, T. E. "Stability of Orthotropic Cylindrical Shells Under Combined Loading" Am. Rocket Society Journal, Vol. 31, No. 2, Feb. 1961, pp. 237-246.
24. Kobayashi, S., Koyama, K., and Seko, H., "Compressive Buckling of Graphite-Epoxy Composite Circular Cylindrical Shells" (Abstract and Supplement of Abstract), Paper presented at the AIAA/ASME/ASCE/AHS 23rd Structures, Structural Dynamics, and Materials Conference, New Orleans May 1982; also private communications.
25. Booton, N., "Buckling of Imperfect Anisotropic Cylinders Under Combined Loading" UTIAS Report No. 203, University of Toronto, August 1976; also Proceedings of AIAA/ASME/ASCE/AHS Structures, Structural Dynamics and Materials Conference, Bethesda, Md.

26. Tennyson, R. C., and Muggeridge, D. B., "Buckling of Laminated Anisotropic Imperfect Circular Cylinders under Axial Compression" J. Spacecraft and Rockets, Vol. 10, No. 2, Feb. 1973, pp. 143-148.